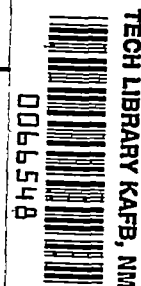


776
NACA TN 3494



NATIONAL ADVISORY COMMITTEE FOR AERONAUTICS

TECHNICAL NOTE 3494

SOUND PROPAGATION INTO THE SHADOW ZONE IN A
TEMPERATURE-STRATIFIED ATMOSPHERE
ABOVE A PLANE BOUNDARY

By David C. Pridmore-Brown and Uno Ingard
Massachusetts Institute of Technology



Washington
October 1955

AFM 3

TECHNICAL
NOTE



TECHNICAL NOTE 3494

SOUND PROPAGATION INTO THE SHADOW ZONE IN A
TEMPERATURE-STRATIFIED ATMOSPHERE
ABOVE A PLANE BOUNDARY

By David C. Pridmore-Brown and Uno Ingard

SUMMARY

The investigation presented herein of the sound field about a point source over a plane boundary in the presence of a vertical temperature gradient represents one phase of a general program of research in atmospheric acoustics.

In this report geometrical ray acoustics is employed to derive the ray paths and the intensity distribution about a source located in a uniformly stratified medium. A comparison of the relative effect of the stratification on the intensity from a directive source and from a spherical source is made.

Also presented is a theoretical analysis of the sound field in the "shadow zone" (diffraction region) formed over an absorbing plane boundary in a temperature-stratified atmosphere. The analysis holds for both two and three dimensions. The boundary condition at the plane is given by a normal acoustic impedance independent of the angle of incidence. As in the corresponding problem of underwater sound where the boundary is a pressure-release surface, it is found that the major portion of the sound intensity in the shadow region decays exponentially with distance at a rate proportional to the one-third power of frequency and to the two-thirds power of temperature gradient. The effect of ground impedance enters mainly through its resistive component. The rate of sound decay for a pressure-release boundary (zero impedance) is found to be 2.3 times that for a reflecting boundary (infinite impedance).

Finally the results of measurements of the sound distribution in a two-dimensional laboratory chamber in which a large temperature gradient was created are reported. Measurements were made at various frequencies for both reflecting and absorbing boundaries, and the results are found to be in good agreement with theory.

INTRODUCTION

A study of the propagation of sound in the atmosphere must take account of the fact that the medium is, in general, neither homogeneous nor quiescent. The principal atmospheric factors affecting sound propagation seem to be humidity, turbulence, and wind and temperature gradients (ref. 1). In addition to these, the effect of the ground must be considered (ref. 2). With the exception of humidity, the effect of which is generally small, these factors are clearly interrelated, the strength of one being somewhat dependent on the presence of the others.

The presence of turbulence causes attenuation of sound as a result of a scattering of the sound energy, the attenuation increasing with frequency and wind velocity. Turbulence has generally been considered the factor of major importance among those mentioned (ref. 3), although no systematic study of it seems to have been made. The existence of wind and temperature gradients is evidenced in the continuous refraction of the acoustic rays or energy paths. This continuous refraction in itself, has little influence on the sound intensity; however, the effect of refraction in attenuating sound may be greatly enhanced, often exceeding that of turbulence, owing to a peculiar influence of the ground boundary resulting in "shadow formation" as illustrated in figure 1. This phenomenon, which has been realized and studied in some detail in the field of underwater sound, seems to have been overlooked in the atmosphere. However, unpublished field measurements obtained at the Massachusetts Institute of Technology have clearly shown the importance of shadow formation, and the present detailed study of the sound field in the temperature-created shadow zone was suggested by these observations.

This investigation was conducted at M.I.T. under the sponsorship and with the financial assistance of the National Advisory Committee for Aeronautics.

SYMBOLS

b	frequency parameter, $\beta c_0 / T_0 \omega$
c	sound velocity, function of z
c_0	sound velocity at ground
H	"height" of atmosphere
$H_n^{(2)}(x)$	Hankel function of second kind of order n

h source height

I intensity

$J_n(x)$ Bessel function of order n

k propagation constant

L total power output

$$Q^2 = \frac{\omega^2}{c^2} - k^2$$

r radial coordinate, distance from source

r_0 distance from source at height h to shadow boundary at height z

T_0 absolute temperature at ground

t_0 travel time from source at height h to shadow boundary at height z

$$u = \int_{z_0}^z Q \, dz$$

$$u_0 = \int_{z_0}^0 Q \, dz$$

$$v = u_0 e^{-i\pi}$$

Z acoustic impedance of ground

$Z_{1/3}(u)$ linear combination of one-third order Bessel functions

z vertical coordinate, receiver height

z_0 first-order zero of Q , $Q(z_0) = 0$

α sound velocity gradient

β temperature gradient

ξ	impedance ratio of ground, $Z/\rho_0 c_0$
η	admittance ratio, $1/\xi$
θ	resistive component of impedance ratio
ρ	density of air
ρ_0	density of air at ground
τ	defined by $k = \frac{\omega}{c_0} \cos \tau$
ϕ	velocity potential

RAY ACOUSTICS

For many problems involving the sound field about a source in a nonhomogeneous medium the high-frequency approximation afforded by geometrical (ray) acoustics is sufficient. Unless only qualitative results are desired, however, the method becomes impractical in the neighborhood of reflecting boundaries, and it clearly fails inside a shadow zone. In the case of a sound field from a spherical source, ray acoustics predicts very small effects from the temperature gradients which are normally encountered in the atmosphere. Thus, for instance, the normal adiabatic lapse rate of 1°C per 100 meters causes a sound diminution in the horizontal direction of only $10^{-4} r^2$ decibels (r in kilometers) in addition to the diminution indicated by the inverse-square law for short ranges. There is, however, one case amenable to ray acoustics where a temperature gradient can have quite a significant influence on a sound field and that is when the source is directive.

The path of a sound ray is determined directly by Fermat's principle which requires that the path be such that the time of traversal is a minimum (or extremum). This condition is met by requiring that the integral $\int \frac{ds}{c}$ be stationary or, expressed symbolically, that $\delta \int \frac{ds}{c} = 0$,

where ds is an element of the path, c is the velocity at that point, and δ is the conventional symbol for the variation of a functional. It is assumed that c is a function of one coordinate only, namely, $c(z)$, so that $ds = \sqrt{1 + (r')^2} dz$, where $r' = dr/dz$. The Euler equation corresponding to the problem

$$\delta \int \frac{\sqrt{1 + (r')^2}}{c(z)} dz = 0$$

is

$$\frac{d}{dz} \left[c(z)^{-1} \frac{r'}{\sqrt{1 + (r')^2}} \right] = 0$$

whence,

$$\frac{(r')^2}{1 + (r')^2} = \frac{c^2}{A^2}$$

where A is a constant. The general equation for the ray path is then

$$r = \int \frac{c(z) dz}{\sqrt{A^2 - c^2}} \quad (1)$$

Putting $\frac{dz}{dr} = \tan \theta$, where θ is the angle of inclination of the ray, gives

$$A = \frac{c(z)}{\cos \theta}$$

which is Snell's law. Thus, in the integrand in equation (1), A plays the role of a ray parameter. The integration of this equation yields circular paths for a constant velocity gradient and cycloids for a velocity gradient proportional to the square root of one coordinate (constant temperature gradient).

Distance to Shadow Zone

Consider a source to be located a height h above ground (at $z = 0$) and suppose the sound velocity to diminish with height. Those rays which just graze the earth, that is, which have zero slope at $z = 0$, then define a bounding surface (in three dimensions) separating the sound region from the shadow region. For these rays, clearly the ray parameter A equals c_0 , with c_0 the velocity at the ground. The horizontal distance between a source located at $z = h$ and the start of the shadow zone is then

$$r(h) = \int_0^h \frac{c(z) dz}{\sqrt{c_0^2 - c(z)^2}} \quad (2)$$

If the receiver is located at a height z on the shadow boundary, then the horizontal distance from source to receiver is

$$r_0 = r(h) + r(z)$$

For a constant gradient of velocity, $c(z) = c_0 - \alpha z$ and

$$r(h) = \frac{c_0}{\alpha} \sqrt{\frac{\alpha h}{c_0} \left(2 - \frac{\alpha h}{c_0} \right)} \approx \sqrt{2 \frac{c_0 h}{\alpha}} \quad (3)$$

For a constant temperature gradient β , $c(z) = c_0 \left[1 - (\beta z / T_0) \right]^{1/2}$ and

$$r(h) = \frac{T_0}{\beta} \left[\sin^{-1} \sqrt{\frac{\beta h}{T_0}} + \sqrt{\frac{\beta h}{T_0} \left(1 - \frac{\beta h}{T_0} \right)} \right] \approx 2 \sqrt{\frac{T_0 h}{\beta}} \quad (4)$$

The approximations hold for small values of the gradient. Equation (4) has been plotted in figure 2 for the case in which source and receiver are at the same height.

The travel time t_0 of the ray from source to shadow boundary is discussed subsequently. This time may be broken up into $t_0 = t(h) + t(z)$, where

$$t(h) = \int \frac{ds}{c} = \int \frac{\sqrt{1 + (r')^2}}{c(z)} dz = \int \frac{c_0/c}{\sqrt{c_0^2 - c^2}} dz$$

The value of r' has been substituted from equation (2). For a constant temperature gradient,

$$t(h) = \frac{2T_0}{c_0\beta} \sin^{-1} \sqrt{\frac{\beta h}{T_0}} \quad (5)$$

Intensity Distribution

Once the paths of the sound rays have been determined, it is a simple matter, as shown in reference 5, to calculate the intensity distribution by considering the geometrical divergence of these rays. Thus, consider a spherical source with a total power output L . The intensity on a small sphere of radius a centered on the source is then $L/4\pi a^2$. Consider now two neighboring rays leaving the source at angles of elevation ϕ_0 and $\phi_0 + \delta\phi_0$. Then, through the space bounded by the two surfaces formed by rotating these rays about the z -axis, a certain amount of power

δL flows equal to that which falls on the sphere zone cut out by these rays; that is,

$$\delta L = \frac{L}{4\pi a^2} 2\pi a^2 \cos \phi_0 \delta \phi_0 = \frac{L}{2} \cos \phi_0 \delta \phi_0$$

The intensity I at any point (r, ϕ) is then the ratio of this power δL to the area $2\pi r \delta \sigma$ through which it flows at this distance, $\delta \sigma$ being the perpendicular separation of the rays. Thus,

$$I = \frac{L \cos \phi_0}{4\pi r} \frac{\delta \phi_0}{\delta \sigma} \quad (6)$$

The value of the interval $\delta \sigma$ along the ray remains to be calculated. From figure 3 it can be determined that

$$\begin{aligned} \delta \sigma &= \sin \phi \delta r \\ &= \sin \phi \delta \int dr \\ &= \sin \phi \delta \int \cot \phi dz \\ &= -\sin \phi \int \frac{\delta \phi}{\sin^2 \phi} dz \end{aligned}$$

The quantities $\delta \phi$ and dz appearing in the integrand may be computed from Snell's law, which reads

$$\begin{aligned} \frac{\cos \phi}{\cos \phi_0} &= \frac{c(z)}{c_0} \\ \frac{\cos(\phi + \delta \phi)}{\cos(\phi_0 + \delta \phi_0)} &= \frac{c + \delta c}{c_0} \end{aligned}$$

Neglecting δc and expanding the cosine gives

$$(\tan \phi) \delta \phi = (\tan \phi_0) \delta \phi_0 \quad (7)$$

Differentiating Snell's equation gives

$$dz = - \frac{c}{c' \tan \phi} \frac{d\phi}{\delta \phi} \quad (8)$$

where $c' = \frac{dc}{dz}$. Combining equations (7) and (8) gives finally

$$\delta\sigma = -\sin\phi \tan\phi_0 \delta\phi_0 \int \frac{c \, d\phi}{c' \sin^2\phi} \quad (9)$$

These results are now applied to the case of a constant temperature gradient. For simplicity the source and receiver are assumed to be at

the same height. With $c(z) = c_0 \left(1 + \frac{\beta z}{T_0}\right)^{1/2}$,

$$\frac{1}{c} \frac{dc}{dz} = \frac{1}{2} \frac{\beta}{T_0} \left(\frac{\cos\phi_0}{\cos\phi} \right)^2$$

and equation (8) becomes

$$\begin{aligned} \frac{\delta\sigma}{\delta\phi_0} &= -2 \frac{T_0}{\beta} \frac{\sin\phi \sin\phi_0}{\cos^3\phi_0} \int_{\phi_0}^{\phi} \cot^2\phi \, d\phi \\ &= \frac{2T_0/\beta}{\cos^3\phi_0} \left[\sin(\phi_0 - \phi) - (\phi_0 - \phi) \sin\phi \sin\phi_0 \right] \end{aligned}$$

The value of this quantity at the source height is obtained by putting $\phi = -\phi_0$ (note that the above integral may not be evaluated directly from ϕ_0 to $-\phi_0$ since it diverges); whence,

$$\frac{\delta\sigma}{\delta\phi_0} = \frac{4T_0}{\beta} \frac{\sin\phi_0}{\cos^2\phi_0} \left(1 + \phi_0 \tan\phi_0 \right) \quad (\phi = -\phi_0) \quad (10)$$

The horizontal distance r from source to receiver (at the source height) may be expressed in terms of ϕ_0 as

$$r = \int \cot\phi \, dz = -2 \int_{\phi_0}^0 \frac{c}{c'} \, d\phi = \frac{T_0}{\beta \cos^2\phi_0} (2\phi_0 + \sin 2\phi_0) \quad (11)$$

Here, use has been made of the differentiated form of Snell's law, equation (8). In terms of I_0 , the intensity from the same source in a

homogeneous medium ($I_0 = \frac{L}{4\pi r^2}$), the excess attenuation due to the inhomogeneity is obtained from equations (6) to (10) as

$$\frac{I}{I_0} = \frac{1}{4} \frac{2\phi_0 + \sin 2\phi_0}{\tan \phi_0 (1 + \phi_0 \tan \phi_0)} \quad (12)$$

where ϕ_0 is related to r in equation (11). For small values of $\beta r/T_0$ equations (11) and (12) combine to give

$$\frac{I}{I_0} \approx 1 - \frac{1}{12} \left(\frac{\beta r}{T_0} \right)^2$$

For a source I' with a directivity pattern $f(\phi_0)$,

$$\left(\frac{I}{I_0} \right)' = \frac{I}{I_0} \frac{f(\phi_0)}{f(0)} \quad (13)$$

The relative effect of a temperature gradient on a spherical source and on a directive one is illustrated in figure 4, where equations (12) and (13) have been plotted as a function of the distance parameter $\beta r/T_0$ from equation (11) for a simple source. The second curve is for a dipole source oriented at 45° to the horizontal, $f(\phi_0) = \cos[\phi_0 - (\pi/4)]$. It is seen that out to a distance of $\frac{\beta r}{T_0} \approx 1.8$ (about 5 kilometers for the normal adiabatic lapse rate) the effect of the temperature gradient is to increase the sound received from the dipole source but to diminish that from the spherical one. Unless a temperature inversion prevails, a shadow zone may, of course, begin to form before this point.

DIFFRACTION INTO SHADOW ZONE

In order to derive an expression for the sound distribution within an acoustic shadow zone brought about by a temperature stratification of the medium above a plane boundary, several approaches are discussed and evaluated. In one approach the formal Green's function solution to the wave equation in such a medium is derived as a series of normal modes. The fundamental but involved method of contour integration presented by Pekeris is discussed briefly and compared with the Green's function method, the case of a medium with a constant (acoustic) velocity gradient being used as a basis for comparison. Finally, an approximate solution is presented for the case in which a constant gradient of temperature exists in the medium. The rapid convergence of this solution in the shadow zone is such that the behavior of the sound field within this region is adequately expressed by the first mode in the series.

Formal Solution

Consider a spherical source of sound which is driven at a constant frequency $f = \omega/2\pi$, located a distance h above a ground boundary at $z = 0$, and assumed acoustically described by a normal impedance Z , independent of the angle of incidence. Suppose the medium to be stratified so that the sound velocity is a function of the one coordinate z .

The sound field may then be derived from a velocity potential $\phi e^{i\omega t}$ satisfying the wave equation

$$\nabla^2 \phi + \frac{\omega^2}{c(z)^2} \phi = 0 \quad (14)$$

outside the source.

The use of this equation entails two approximations from the outset, namely, the usual one that small amplitudes are required and, also, that the fractional change in any property of the medium must be small in the distance of a wavelength (see appendix A). The latter condition is a restriction to high frequencies but is not stringent even for the very high temperature gradients which were created artificially in the model weather chamber to be described subsequently. For example, if $\delta\lambda$ is written for the change in wavelength in the distance of a wavelength, then the requirement $(\delta\lambda/\lambda) \ll 1$ is equivalent to $(\alpha/f) \ll 1$ where

$\alpha = \frac{dc}{dz}$ is the velocity gradient. In practice α is of the order of 0.01 second^{-1} for a stable (adiabatic) atmosphere while, in the chamber, values as high as 120 second^{-1} were produced.

Equation (14) can always be separated in cylindrical coordinates by putting $\phi(r, z) = R(r)F(z)$, which gives

$$\frac{1}{r} \left(\frac{d}{dr} r \frac{dR}{dr} \right) + k^2 R = 0 \quad (15)$$

and

$$\frac{d^2 F}{dz^2} + \left[\frac{\omega^2}{c(z)^2} - k^2 \right] F = 0 \quad (16)$$

where k^2 is the separation constant. Now, if it is assumed that (1) the velocity $c(z)$ is a continuous monotonic function of z such

that $c(0) = c_0$ and $c(H) = 0$, that (2) at $z = 0$ the boundary condition is $\frac{F}{dF/dz} = \frac{Z}{i\omega\rho}$, and that (3) for large values of z the solution represents upgoing waves, a set of eigenfunctions $F_m(z)$ and corresponding eigenvalues k_m may be determined based upon these assumptions. The solution to the problem may then be expressed in the following equation as an infinite sum of these eigenfunctions with undetermined coefficients:

$$\phi = \sum_m A_m H_0^{(2)}(k_m r) F_m(z) \quad (17)$$

Here, $H_0^{(2)}(k_m r)$ is chosen as the solution to equation (15) in order to insure outgoing waves in conjunction with the time factor $e^{i\omega t}$. In order to evaluate the coefficients A_m equation (14) must be rewritten, introducing a source term on the right corresponding to a point source at $r = 0$, $z = h$, as follows:

$$\nabla^2 \phi + \frac{\omega^2}{c(z)^2} \phi = -\frac{2}{r} \delta(r) \delta(z - h) \quad (18)$$

Here, δ stands for the "delta" function. Substituting equation (17) into equation (18) and making use of equation (16) lead to

$$\left\{ \frac{1}{r} \frac{d}{dr} \left[r \frac{d}{dr} H_0^{(2)}(k_m r) \right] + k_m^2 H_0^{(2)}(k_m r) \right\} A_m F_m(z) = -\frac{2}{r} \delta(r) \delta(z - h)$$

Now, multiply both sides of this equation by $F_n(z)$ and integrate over the surface of a small cylinder enclosing the source. Because of the orthogonality of the functions, it is possible to obtain the following equation:

$$\begin{aligned} \frac{-4\pi F_m(h)}{\int_0^H F_m^2(z) dz} &= 2\pi A_m r \frac{d}{dr} H_0^{(2)}(k_m r) \\ &= -2\pi A_m k_m r H_1^{(2)}(k_m r) \end{aligned}$$

As $r \rightarrow 0$,

$$\frac{-4\pi F_m(h)}{\int_0^H F_m^2(z) dz} \rightarrow -4iA_m$$

The solution is, then,

$$\phi e^{i\omega t} = -i\pi e^{i\omega t} \sum_{m=1}^{\infty} \frac{H_0^{(2)}(k_m r) F_m(h) F_m(z)}{\int_0^H F_m^2(z) dz} \quad (19)$$

where $\frac{F_m}{dF_m/dz} = \frac{z}{i\omega\rho}$ at $z = 0$.

In two dimensions (x, z) the solution follows the same pattern; thus,

$$\phi = -2\pi i \sum_{m=1}^{\infty} \frac{e^{-ik_m |x|} F_m(h) F_m(z)}{k_m \int_0^H F_m^2(z) dz} \quad (20)$$

with the same boundary conditions on F .

The functions F_m depend on the velocity profile $c(z)$ and the boundary conditions at the ground. Two cases are now considered, one in which the velocity $c(z)$ diminishes proportionally with the height (constant velocity gradient) and the other in which it diminishes with the square root of the height.

Medium With Constant Velocity Gradient

Equation (14) has been solved in reference 6 for the case of a source located underwater with $c(z) = \alpha z$. In accordance with the notation of reference 6, reverse the sign of the z -coordinate and assume the source to be located at $z = \sigma$ and the ground at $z = \gamma$. The eigenfunction solutions to equation (16) are then

$$F_m(z) = z^{1/2} J_{in}(ik_m z)$$

where

$$J_{in}(x_m) + \frac{2x_m}{1 + 2i \frac{\omega}{\alpha}} J'(x_m) = 0 \quad (21)$$

Here $n = \left(\frac{\omega^2}{\alpha^2} - \frac{1}{4} \right)^{1/2}$, $\eta = \frac{\rho_o c_o}{Z}$, and $x_m = ik_m \gamma$. The general solution, equation (19), then takes the form

$$\phi = -2i\pi \frac{(\sigma z)^{1/2}}{\gamma^2} \sum_m \frac{H_o^{(2)}(k_m r) J_{in}(ik_m \sigma) J_{in}(ik_m z)}{\left[1 + \left(n^2 / x_m^2 \right) \right] J_{in}^2(x_m) + (J_{in}')^2(x_m)} \quad (22)$$

For a pressure release at the boundary, $\eta \rightarrow \infty$ and $J_{in}(x_m) = 0$, in which case equation (22) comes under Pekeris' solution.

Discussion of method of solution.— It is perhaps worthwhile at this point to give a brief summary of the method used by Pekeris to arrive at his solution in order to compare it with the method of normal modes employed herein. Pekeris starts from the wave equation (without a source term) and divides the medium into two regions, one above the source and the other below. The function F is expressed as a linear combination of the functions $z^{1/2} I_{in}(kz)$ and $z^{1/2} K_{in}(kz)$ in each region, I and K being the modified Bessel functions. The four arbitrary constants involved are then determined (1) by the boundary condition at the water surface, (2) by the requirement that the pressure be continuous across the interface of the two regions, (3) by the requirement that at great depths the solution represent a downgoing wave, and (4) by the source strength. In this way the solution is expressed as an integral over the separation constant k as

$$\phi = \int_0^\infty J_o(kr) F(z) k \, dk \quad (23)$$

the path of integration being determined to satisfy the source condition,

that is, such that $-\int \phi \, dS = 4\pi q$, where q is the source strength.

An investigation of the behavior of the integrand in the complex k -plane reveals that it is free of branch points but that it possesses poles and that these are all situated in the fourth quadrant. The integral in equation (23) is then split into two integrals by writing

$J_0(kr) = \frac{1}{2} \left[H_0^{(1)}(kr) + H_0^{(2)}(kr) \right]$, and the path of integration of the

new integrals is deformed to enclose the first and fourth quadrants, respectively. This procedure results in the solution being expressed as a sum of residues taken at the poles of the integrand in the fourth quadrant together with two integrals taken respectively over the positive and negative imaginary axes. These two integrals can be shown to cancel each other, and the remaining sum of residues is equivalent to equation (22) with $J_{in}(x_m) = 0$ at $\eta = \infty$.

This method of solution is clearly tedious since for each case it must be ascertained whether branch points exist, that the integrals taken along the infinite axes vanish, and that the remaining integrals over the imaginary axes cancel. From the theory of normal modes these conditions would be expected to hold automatically. That the theory does not preclude the possibility of the existence of branch points but only requires that they shall not contribute to the solution is illustrated by the case

where $c(z) = c_0 / (1 + \alpha z)^{1/2}$, which is also discussed by Pekeris. The integrand corresponding to equation (23) now contains three branch points, and the solution includes an additional branch line integral. However, by a detailed examination of the phase changes of this branch line integrand as it is taken around the branch cut Pekeris is able to show that its contribution is zero. The use of Pekeris' method, then, would seem to be dictated only in cases where the normal-mode theory breaks down. This occurs whenever the function F or its derivative is discontinuous, for then the necessary orthogonality relation which normally results from equation (16), namely,

$$\left(F_m F_n - F_m' F_n' \right)_{z=0}^{z=H} = 0 = (k_m^2 - k_n^2) \int_0^H F_m F_n dz \quad (24)$$

no longer holds. In practice the first derivative must, of course, always be continuous (continuity of velocity), but a discontinuity in the density will make F discontinuous (continuity of pressure). Again, if there is a discontinuity in the sound velocity $c(z)$, the eigenfunctions F_m do not form a complete set (ref. 7) although they are still orthogonal; however, equation (24) still holds since only the second derivative is affected. In all of these cases the solution must include a branch line integral. In a homogeneous (infinite) medium this will be the entire solution since then there are no modes (continuous spectrum).

Asymptotic solution.— In an appendix to reference 6 Pekeris derives an asymptotic expression for the imaginary-order Bessel functions appearing in the solution of equation (22) herein which is valid for

high frequencies ($n \approx \frac{\omega}{\alpha}$ large). Use is made of this expression to arrive at a general relation for the roots of equation (21) valid for an arbitrary boundary.

In the limit of large values of n reference 6 shows that asymptotically

$$J_{in}(x) \sim \left(\frac{-2i}{\pi n T}\right)^{1/2} \cos\left(\theta - \frac{\pi}{4}\right) \quad (25)$$

where

$$\theta = \text{in}(T - \tan^{-1}T)$$

$$T = -i \left[1 + \left(x^2/n^2 \right) \right]^{1/2}$$

Since the value of T is small (at the roots it is proportional to $\frac{c_0}{\omega} Q_0$ presented subsequently and it varies as $f^{-1/3}$ for high frequencies), the inverse tangent may be expanded as follows:

$$\theta = \text{in}\left(\frac{1}{3} T^3 - \frac{1}{5} T^5 + \dots\right)$$

Retaining only the first term gives

$$\theta \approx \frac{1}{3} \text{in} T^3 = -\frac{1}{3} n \left[1 + \left(x^2/n^2 \right) \right]^{3/2}$$

or

$$x_m = ik_m \gamma = \text{in} + A_m n^{1/3} e^{i\pi/6} + \dots \quad (26)$$

where $A_m = \frac{1}{2} (3\theta_m)^{2/3}$. This expression holds only at the boundary $z = \gamma$, since elsewhere T need not be small.

Now, the Hankel function appearing in equation (22) is represented asymptotically (large value of r) by

$$H_0^{(2)}(k_m r) \sim \sqrt{\frac{2}{\pi k_m r}} e^{-i(k_m r - \frac{\pi}{4})}$$

Since the roots from equation (26) have a positive imaginary part, this clearly leads to an exponential decay at large distances from the source.

The rate of decay in decibels is $\left(8.68 \frac{\sqrt{3}}{2} A_m n^{1/3}\right)/\gamma$ decibels per meter for each mode. It is thus proportional to the one-third power of the frequency and to a constant value of A_m , which is now determined from the boundary impedance.

Introducing the asymptotic expression (25) into equation (21) to obtain the roots and writing $B^{-1} = 1 + 2i\eta(\omega/\alpha)$ give

$$\cot\left(\theta - \frac{\pi}{4}\right) = \frac{2inT^3}{T^2 + B(x^2/n^2)} \quad (27)$$

For a pressure release, $B = 0$ and $\theta_m = \pi\left[m - (1/4)\right]$. This is the case which Pekeris treated and leads to $A_1 = 1.85$, $A_2 = 3.24$,

For a ρc boundary $B^{-1} = 1 + 2i(\omega/\alpha) \approx 2in$ and

$$\cot\left(\theta - \frac{\pi}{4}\right) = \frac{T^3}{T^2 + (x^2/2in^3)} = \left(\frac{3\theta}{in}\right)^{1/3} \left[1 + \frac{1}{2}(3\theta)^{-2/3} n^{-1/3} e^{-i\pi/6} \dots\right]$$

This gives approximately

$$\theta_m = \pi\left(m - \frac{1}{4}\right) - \left(\frac{3\theta_m}{in}\right)^{1/3}$$

for large values of n . Thus, in this case, the root depends slightly on the frequency but may always be ascertained for any given frequency by iteration, that is, by inserting the value $\pi\left[m - (1/4)\right]$ for θ_m on the right to obtain a second approximation, and so forth.

For a hard boundary, $B = 1$ and equation (27) reduces to

$$\begin{aligned} \cot\left(\theta - \frac{\pi}{4}\right) &= \frac{2inT^3}{T^2 + (x^2/n^2)} = -2inT^3 \\ &= -6\theta \left[1 + \frac{1}{5} 3^{5/3} \left(\frac{\theta}{n}\right)^{2/3} e^{-i\pi/3} \dots\right] \end{aligned}$$

This gives $\theta_1 = 0.365$, $\theta_2 = 3.88$, and $\theta_m = \pi[m - (3/4)]$, with $m \geq 3$; whence, $A_1 = 0.53$ and $A_2 = 2.57$.

Numerical examples.— At large distances from the source the first mode is clearly the only surviving one. As an example, take $\alpha = 0.01 \text{ second}^{-1}$, which is a typical atmospheric value. At 500 cps the decay rates for the first mode are 44 db/mile for $Z = 0$, 43 db/mile for $Z = \rho c$, and 12.5 db/mile for $Z = \infty$. As a second example, take $\alpha = 100 \text{ seconds}^{-1}$, $f = 10,000 \text{ cps}$, and $c_0 = 420 \text{ m/sec}$. The decay rates for this case are 8.6 db/foot for $Z = 0$, 8.4 db/foot for $Z = \rho c$, and 2.6 db/foot for $Z = \infty$.

Medium With a Constant Temperature Gradient

In a medium with a constant temperature gradient the velocity function is

$$c(z) = c_0 [1 - (\beta z / T_0)]^{1/2}$$

where T_0 is the absolute temperature at the ground and $\beta = dT/dz$ is the temperature gradient. To obtain a solution to equation (16) a method proposed by Langer (ref. 8) is adopted. Langer shows that

$$\frac{d^2 F}{dz^2} + (Q^2 - \theta)F = 0$$

where

$$\theta = \frac{3}{4} \left(\frac{Q'}{Q} \right)^2 - \frac{1}{2} \frac{Q''}{Q} - \frac{5}{36} \left(\frac{Q}{u} \right)^2$$

has the exact solution

$$F = \sqrt{(u/Q)} Z_{1/3}(u) \quad (28)$$

in which

$$u = \int_{z_0}^z Q \, dz$$

$Z_{1/3}$ linear combination of Bessel functions

z_0 first-order zero of Q

These solutions given in equation (28) are a good approximation to the actual solutions of equation (16) provided that $Q^2 \gg \theta$. Now, in this case, with $Q^2 = \omega^2 / c(z)^2 - k^2$ the term θ becomes (see appendix B; symbol O means "order of")

$$\theta = -\frac{3}{16} \frac{1}{H^2} \left(\frac{c_0}{c}\right)^4 + O\left(\frac{Q^2 c_0^4}{\omega^2 c^2 H^2}\right) + \dots$$

with $H = T_0/\beta$. Also, it appears from equation (39) of the body of the text and equation (46) of appendix C that for high frequencies

$$Q_0^2 \approx \left(3u_0\omega^2/2Hc_0^2\right)^{2/3}$$

The condition $Q^2 \gg \theta$ may then be replaced by

$$(\omega H/c_0) \gg 1 \quad (29)$$

This restriction, however, is essentially the same as that already assumed in order for the wave equation (eq. (14)) to be valid, since $f/\alpha \approx \omega T_0/(\pi c_0 \beta)$ where $\alpha = dc/dz$.

In terms of these functions, the solution given in equation (19) takes the form

$$\phi = -i\pi \sum_{m=1}^{\infty} \left(\frac{uu_1}{QQ_1}\right)^{1/2} \frac{H_0^{(2)}(k_m r) H_{1/3}^{(2)}(u_1) H_{1/3}^{(2)}(u)}{\int_0^H (u/Q) \left[H_{1/3}^{(2)}(u) \right]^2 dz} \quad (30)$$

where the eigenvalues k_m are obtained from

$$-\frac{i\omega\rho}{Z} \left(\frac{u_0}{Q_0}\right)^{1/2} H_{1/3}^{(2)}(u_0) = \frac{d}{dz} \left[\left(\frac{u}{Q}\right)^{1/2} H_{1/3}^{(2)}(u) \right]_{z=0} \quad (31)$$

Here, $u_m(z=0) = u_0$, $u_m(h) = u_1$, and $u_m(z) = u$; similar expressions are obtained for Q . For the functions $c(z)$ chosen,

$$Q^2 = \frac{\omega^2}{c_o^2 \left(1 - \frac{z}{H}\right)} - k^2 \quad (H = T_o/\beta) \quad (32)$$

and

$$u = \int Q \, dz = \left(\omega^2 H / c_o^2 k\right) \tan^{-1}(Q/k) - (H - z)Q \quad (33)$$

The substitution $Q = k \tan \tau$ reduces equation (33) to the form

$$\frac{\tau}{\cos \tau} - \sin \tau + \left(\frac{c_o}{\omega H}\right)v_m = 0 \quad (34)$$

with

$$v_m = u_o e^{-i\pi}$$

Also, it is shown in appendix C that equation (31) may be approximated by

$$f(v_m) \equiv \frac{J_{1/3}(v_m) + J_{-1/3}(v_m)}{J_{2/3}(v_m) - J_{-2/3}(v_m)} = \frac{-iZ}{\rho_o c_o} \sin \tau \quad (35)$$

For the higher modes the expression on the left is conveniently replaced by $\cot\left[v_m - (\pi/4)\right]$. The determination of the roots of equation (31) then involves the simultaneous solution of equations (34) and (35). Before solving these equations, however, it is instructive to examine the general solution in the limit of high frequencies and so gain a better insight into the diffraction mechanism.

Behavior of solution at high frequencies.—The quantities u , u_1 , Q , and Q_1 appearing in the general solution, equation (30), are related in equations (32) and (33). From equation (34) it is clear that τ is small in the high-frequency range. Accordingly, put

$$k_m = (\omega/c_o) \cos \tau = (\omega/c_o)(1 + \delta_m) \quad (36)$$

Then, to the first order in δ_m ,

$$Q \approx (\omega/c) \left[(z/H)^{1/2} - \delta_m (c/c_0)^2 (H/z)^{1/2} \right]$$

where the approximation holds provided $(z/H) \gg \delta_m$. Similarly,

$$\tan^{-1}\left(\frac{Q}{k}\right) \approx \tan^{-1}\left(\frac{c_0}{c} \sqrt{\frac{z}{H}}\right) - \frac{(H/z)^{1/2} \delta_m (c_0/c)}{1 + (z/H)(c_0/c)^2}$$

Introducing these expressions into equation (33) gives to the first order in δ_m (note that $\tan^{-1}(zc_0^2/Hc^2)^{1/2} = \sin^{-1}(z/H)^{1/2}$)

$$u_m(z) \approx (\omega H/c_0) \left\{ \sin^{-1}(z/H)^{1/2} - (z/H)^{1/2} [1 - (z/H)]^{1/2} \right\} - \delta_m (\omega H/c_0) \left\{ \sin^{-1}(z/H)^{1/2} + (z/H)^{1/2} [1 - (z/H)]^{1/2} \right\}$$

The first term in this phase factor is recognized as the one obtained directly from ray acoustics, namely, $\omega \left\{ t'(z) - [r'(z)/c_0] \right\}$, in which

$$\left. \begin{aligned} r'(z) &= H \left\{ \sin^{-1}(z/H) + (z/H)^{1/2} [1 - (z/H)]^{1/2} \right\} \\ t'(z) &= (2H/c_0) \sin^{-1}(z/H)^{1/2} \end{aligned} \right\} \quad (37)$$

The quantities $r_0 = r'(h) + r'(z)$ and $t_0 = t'(h) + t'(z)$ are then the distance and travel time, respectively, of a ray from the source at height h to a point at height z on the shadow boundary. The small coefficient δ_m of the second term in the phase factor u is complex and leads to attenuation when r is greater than the shadow distance r_0 . This is seen by replacing the Hankel functions appearing in solution (30) by their asymptotic forms and by using equation (37) for u and u_1 to obtain the high-frequency approximation to the general solution

$$\phi e^{i\omega t} \approx \sum_{m=1}^{\infty} B_m \left(\frac{r_0}{r} \right)^{1/2} e^{i\omega \left\{ t - t_0 - \left[(1 + \delta_m)(r - r_0) \right] / c_0 \right\}} \quad (38)$$

where

$$B_m = \frac{2\sqrt{2} e^{7\pi i/12}}{F^2 (\pi k_m Q_1 Q)^{1/2}}$$

Here,

$$F^2 = \int_0^H \frac{u}{Q} \left[H_{1/3}^{(2)}(u) \right]^2 dz \approx \frac{2}{\pi} \int_{u_0}^{u(H)} Q^{-2} e^{-2i \left[u - (5\pi/12) \right]} du$$

The quantity B_m is the pressure amplitude of the m th mode on the shadow boundary $r = r_0$. In two dimensions the factor r_0/r is absent.

The phase of expression (38) gives the time of arrival of each mode at a point in the shadow zone as

$$t = t_0 + \frac{r - r_0}{c_0(1 + \delta_m)}$$

This equation indicates that each mode travels along the downward leg of the limiting ray to the ground and then travels a distance $r - r_0$ along the ground surface before finally reaching the point (r, z) by a path parallel to the upward leg of the limiting ray. This is just what would be expected from Fermat's principle, since the traversal of this path clearly takes the least time. The small frequency-dependent term δ_m leads to dispersion. Its imaginary part is responsible for the attenuation which is seen to take place only over the horizontal stretch along the ground surface.

Rate of decay of sound in diffraction region.— The decay of sound in the shadow region due to diffraction alone is given essentially by the first mode as $8.68 \text{Im}k_1$ decibels per meter since the higher modes attenuate much more rapidly. The propagation constant k has been related to the temperature gradient β , the frequency $f = \omega/2\pi$, and the impedance Z through equations (34) and (35). Since $b = c_0/\omega H$ is small according to the criterion of equation (29), equation (34) reduces approximately to

$$\frac{2}{3} \tau^3 + \frac{1}{5} \tau^5 + bv = 0$$

or, on solving for τ ,

$$\tau \approx \left(-\frac{3}{2}bv\right)^{1/3} + \frac{3}{20}bv \quad (39)$$

Either a high-impedance or a low-impedance approximation to equation (35) may be obtained by expanding the left-hand side in a Taylor's series about the infinite or zero impedance values, respectively. Making use of recursion relations for the Bessel functions in obtaining the successive derivatives of $f(v)$ and setting $f(v_0) = 0$ then give, for the low-impedance boundary,

$$f(v) = v_0 - v - \frac{(v - v_0)^2}{bv_0} + \dots$$

where $v_0 = 2.38$ for the first root. Now, solve for v to obtain approximately

$$v \approx v_0 - f - \frac{f^2}{bv_0} \quad (40)$$

For a high-impedance boundary, put $f(v_\infty) = \infty$ where $v_\infty = 0.685$ and define $g(v) = 1/f(v)$. Proceeding in the same way as before the equation

$$g(v) = v - v_\infty - \frac{(v - v_\infty)^2}{6v_\infty} + \dots$$

is obtained; whence,

$$v \approx v_\infty + g - \frac{g^2}{6v_\infty} \quad (41)$$

Finally, by expanding $\cos \tau$, equation (36) may be replaced by

$$\text{Im } k = -\frac{1}{2} \frac{\omega}{c_0} \text{Im } \tau^2 \quad (42)$$

where $\text{Im } k$ is the imaginary part of k .

Low-impedance boundary.— An expression for τ in terms of $\zeta = Z/\rho_0 c_0$ and v_0 may be obtained by substituting from equation (39) into equation (38) and writing equation (35) as $f = -i\zeta\tau$. This gives

$$\tau^2 = \left(-\frac{3}{2} b v_0\right)^{2/3} + i \zeta b$$

Substituting this into equation (42) gives

$$\text{Im } k = 1.01 \left(\frac{\omega}{c_0}\right)^{1/3} \left(\frac{\beta}{T_0}\right)^{2/3} - \frac{1}{2} \frac{\beta}{T_0} \theta + \dots \quad (43)$$

This series holds in the range $|\zeta|^3 \ll (\omega T_0 / c_0 \beta)$ which under ordinary atmospheric conditions outdoors means $|\zeta| \ll 25$ for frequencies of the order of 100 cps. By including more terms in the Taylor's expansion it can be shown that the coefficient of the next term in the series, proportional to $|\zeta|^2$, vanishes.

High-impedance boundary.— An expression for τ in terms of $\eta = \rho_0 c_0 / Z$ and v_∞ may be obtained by substituting from equation (41) into equation (39) and writing equation (35) as $g = i\eta/\tau$. This gives

$$\tau^2 = \left(-\frac{3}{2} b v_\infty\right)^{2/3} + \frac{2}{3} \frac{i\eta}{v_\infty} \left(-\frac{3}{2} b v_\infty\right)^{1/3}$$

From equation (42),

$$\text{Im } k = 0.44 \left(\frac{\omega}{c_0}\right)^{1/3} \left(\frac{\beta}{T_0}\right)^{2/3} + 0.98 \left(\frac{\omega}{c_0}\right)^{1/3} |\eta| \cos\left(\frac{\pi}{3} - \phi\right) \dots \quad (44)$$

where $\eta = |\eta| e^{-i\phi}$. This series holds in the range $|\zeta|^3 = |\eta|^{-3} \gg \frac{\omega T_0}{c_0 \beta}$ which under ordinary conditions in the outdoor atmosphere means $|\zeta| \gg 25$ for frequencies around 100 cps.

In this connection it is of interest to note that the attenuation constant for a pressure-release boundary (zero impedance) is 2.3 times that for a reflecting boundary (infinite impedance).

Typical numerical example.— Consider a point source located 10 feet above ground and driven at 500 cps in an atmosphere in which temperature decreases with height at the rate of 0.5°C per meter. A receiver located at the same height passes into the diffraction region at a distance of

550 feet. Within this region the sound field behaves like a damped cylindrical wave. In other words, apart from decreasing at the rate of 3 decibels per doubling of distance because of divergence, the sound pressure level is observed, from equation (43), to diminish at the additional rate of 78 decibels per 1,000 feet over a ground with a normal impedance of ρc . If the impedance is $10\rho c$ this rate will be 58 decibels per 1,000 feet. From equation (44), a perfectly hard boundary results in a diminution of 35 decibels per 1,000 feet. Note that the major portion of the sound intensity decays exponentially with distance at a rate proportional to the two-thirds power of the temperature gradient.

LABORATORY MEASUREMENTS

Propagation Chamber

In the study of the sound field in the laboratory it is essential to obtain a high temperature gradient in the region of sound propagation in order to secure a shadow zone within a reasonable distance from the sound source. To this end a three-dimensional propagation chamber was first constructed. It consisted of a wooden box 8 by 4 by 3 feet with acoustically insulated side walls. In order to reduce the presence of air currents the temperature was made to increase with height. The "ground" or hard boundary then consisted of a steel hot plate placed along the top of the chamber while water was circulated through coils in the bottom. The temperature at different heights within the chamber was measured by a series of mercury thermometers, which were shielded against radiation. Average temperature gradients of the order of 80°C per meter were set up within the chamber, but they were far from uniform, being greatest near the hot surface. Acoustic measurements were made by introducing a pure tone into the chamber at one end and then exploring the resultant field near the other with a condenser microphone (Altec 21B) with probe attachment. The probe consisted of a 4-foot Pyrex tube which was inserted into the box through holes in the top. The signal was amplified and measured with a narrow-band wave analyzer (General Radio). Figure 5 is a plot of the intensity obtained as a function of depth, the labels (1), (2), and (3) referring to increasing distances from the speaker, which was driven at 8,700 cps. The presence of a shadow boundary is revealed in the rather sharp drop occurring in the intensity at a depth of about 10 inches. It is also noticed that the depth to this boundary increases with distance from the source as would be expected. The "shadow-zone distance" is in order-of-magnitude agreement with that predicted by ray theory (eq. (4)) for this case.

The crude results obtained with this chamber pointed to the desirability of constructing an improved chamber in which a more stable and uniform temperature gradient could be set up. The final two-dimensional

propagation chamber, shown in figure 6, was found to be satisfactory in these respects. This chamber allows cylindrical waves to propagate between two plane parallel steel plates spaced a distance apart less than half a wavelength. Unwanted reflections are eliminated by means of a lining of sound-absorption material. The chamber is heated on the top and cooled at the bottom so that a vertical temperature gradient is maintained in the propagation region.

The steel plates with the dimensions 8 feet by 3 feet by 5/16 inch are separated 5/8 inch, heat insulated on the outside, and supported vertically in a wooden frame. Five 600-watt heating units are placed along a 6-inch-wide plate which is bolted along the top of the chamber. The bottom is cooled by water circulating through a trough in which the plates rest. The temperature is measured by means of mercury thermometers inserted into metal sleeves which fit into holes bored at 6-inch intervals in one of the steel plates.

A cylindrical source of sound is simulated by a series of 1/8-inch slots around the periphery of a short length of pipe with a 3/4-inch bore and with a loudspeaker at one end. The pipe is inserted through the steel plates at a depth of 4 inches below the hot surface. The sound field is explored with a condenser microphone with probe attachment. The probe consists of a 4-foot steel tube with a 3/16-inch bore and is inserted through holes at 10-inch intervals along the hot plate. These holes are numbered from (1) to (9) starting from the source in figure 6, and plots made of measurements taken through them are numbered correspondingly in the graphs (figs. 9, 11, 13, and 14). The microphone arrangement can be raised or lowered continuously by means of a motor-driven elevator. Figure 7 is a photograph of the chamber and electronic instruments. Consideration was given to the question of what temperature distribution could be predicted in this experimental setup, allowance being made for the temperature dependence of the thermal conductivity of air. Since it is known that the conductivity $\lambda(T)$ increases with temperature, it follows that the temperature gradient in the air space is nonuniform, having larger values in regions of low temperature. The actual distribution is given as the solution of the steady-state heat-flow equation

$$\text{div}[\lambda(T) \text{ grad } T] = 0$$

subject to the appropriate boundary conditions. This solution is worked out in appendix D for a reasonable choice of $\lambda(T)$, and the results are presented in figure 8. The temperature midway between the metal side walls is plotted as a function of distance from the hot surface for different values of the parameter γ which is the ratio of T_0/β , the "height of the atmosphere" to the separation L of the side walls in which a constant gradient of temperature is assumed to exist. The curve

labeled $\gamma = 0$ then corresponds to the case where the side walls have been removed to infinity. It is seen that in all cases the temperature gradient is essentially constant near the hot surface.

Experimental Results

An average temperature gradient of 210° C per meter was maintained in the side walls during the sound measurements. Since it appeared that an inordinately long time would have to be allowed for the chamber to attain a uniform temperature gradient, these measurements were usually taken after about 3 to 4 hours of heating, at which time the gradient at the top was still somewhat higher than the average one (about 250° C per meter).

In the first series of measurements made in the new chamber the source was driven continuously at various frequencies. The results of a typical set of measurements made at 9,250 cps are shown in figure 9. They are qualitatively similar to those obtained in the previous chamber. The sudden rise in the sound pressure level at the hot surface was always observed just as the probe tip reached the hole orifice and is probably due to a diffraction effect.

In all subsequent measurements the speaker was driven by pulses, and the resulting signal from the microphone, suitably amplified and filtered, was then displayed on an oscilloscope screen whose sweep was triggered by the pulse to the speaker. Relative pressure amplitude measurements were made by using an attenuator in series with the oscilloscope to maintain a constant pulse height on the screen. A block diagram of the electronic setup is given in figure 10. Figure 11 shows the results of a series of measurements taken in this way with the speaker driven by 8,000-cps millisecond pulses. The pulse length was clearly not short enough to eliminate interference caused by reflections from the hot surface in the normal region.

To obtain a different picture of the distortion of the sound field by the temperature gradient, the relative times of arrival of the pulses at different points in the chamber were observed on the oscilloscope screen by noting the distance between the beginning of the sweep and the appearance of the pulse. Figures 12(a) and 12(b) show the results of such measurements taken in the chamber when cold and when heated, respectively. The numbers give the arrival times of the pulses in arbitrary units. Surfaces of constant phase have been drawn in by interpolation. The distortion of these surfaces in the heated chamber is apparent.

In order to study the effect of an absorbing boundary on the sound field, a 2-inch layer of glass wool was placed directly under the hot surface. Figure 13 gives the results of measurements taken with this

boundary using millisecond pulses at 8,000 cps, but with the chamber unheated. The increasingly steep drop in the pressure level as the boundary was approached at greater distances from the speaker suggests the shadow-zone effect. It may be explained qualitatively as caused by the increasing impedance mismatch between the wave and the boundary for decreasing angles of incidence and is predicted quantitatively in reference 2.

The measurements reported in figure 14 were taken in order to illustrate the additional sound attenuation brought about by the shadow-zone effect. The curves represent the differences in level obtained between a series of measurements taken at six different frequencies in the unheated chamber and the same series taken in the presence of a temperature gradient. There is a noticeable increase in the slopes of these curves with frequency, although for a given frequency the slopes remain fairly constant with distance from the source. A comparison of these curves with those of figures 9 and 11 shows that the shadow zone has moved in closer to the source as would be expected since the introduction of a 2-inch layer of glass wool has reduced the source height. The curves afford a rather striking illustration of the fact that the influence of a temperature gradient is quite negligible in the normal region but becomes pronounced in the diffraction region.

The form of equation (38) indicates that a more direct comparison between theory and experiment would be possible if the pressure measurements were plotted as a function of distance from the source rather than depth, for such plots should yield straight lines in the diffraction region. Since the experimental setup was not adapted to taking such measurements directly, they had to be obtained from the depth measurements by plotting successively points corresponding to the same depth. To justify this procedure, it was imperative to insure that the source output remained constant over the relatively long periods involved in moving the microphone and elevator from one access hole to the next. This was accomplished by introducing a monitoring microphone near the source. Its position is clear from figures 6, 7, and 10. When this was done, it was found possible to repeat all measurements within a variation of 1 decibel either way.

In figures 15 to 17 the pressure level has been plotted as a function of distance from the source in meters. The curves in figure 15, representing measurements taken at four different depths in the chamber, have been placed one above the other, and the approximate shadow boundary as suggested by the curves themselves has been drawn in as a dashed line. Figures 16 and 17 are plots of pressure amplitude measurements in decibels taken at the source height with the hard and the absorbing boundary, respectively, and at frequencies of 2,700, 5,000, 8,000, and 10,400 cps. In the shadow zone in both figures the level is observed to decrease linearly with distance from the shadow-zone boundary.

The theory given previously predicts that as the distance from the shadow boundary increases the behavior of the sound field is given by the first mode, which decays at the rate of $8.68 \text{ Im}k_1$ decibels per unit of length. In order to compare the results in figures 16 and 17 with the theory, assume for the temperature gradient the value prevailing at the top of the chamber, namely, $\beta = 250^\circ \text{ C per meter}$, since the rays are confined to this region. Correspondingly, $T_0 = 450^\circ \text{ C}$ and $c_0 = 420 \text{ meters per second}$. The following decay rates are then obtained for the hard boundary and are compared with the measured slopes in figure 16:

Frequency, cps	Predicted, db/m	Measured, db/m
2,700	8.8	10
5,000	10.8	14
8,000	12.7	$16\frac{1}{2}$
10,400	13.8	$19\frac{1}{2}$

If a pc impedance is assumed for the porous layer, the following values are obtained from figure 17:

Frequency, cps	Predicted, db/m	Measured, db/m
2,700	19.5	19
5,000	24.0	23
8,000	28.1	27
10,400	30.7	29

These measurements were repeatable to within ± 1 decibel. The agreement is remarkably good for the soft-boundary case. Measured values with the hard boundary are somewhat greater than those predicted on the assumption of an infinite impedance, but this is probably to be expected since in practice the impedance is always lowered by the presence of a viscous boundary layer.

Figure 18 is a logarithmic plot of these decay curves as a function of the frequency, which from the first terms of equations (43) and (44) should be straight lines of slope $1/3$. This is again well confirmed in the soft-boundary case. The slope for the hard-boundary case is somewhat greater than $1/3$. This is presumably explained as a contribution from a finite admittance, due to viscosity and heat conduction, which is significant for grazing angles of incidence.

CONCLUDING REMARKS

A theoretical and experimental study of the sound field about a point source over a plane boundary in the presence of a vertical temperature gradient has been made. Results of this study indicate that the existence of a temperature gradient, which by itself leads only to a simple refraction of the sound rays, can in conjunction with the ground boundary result in the formation of a "shadow zone." In the near field (normal region) the effect of the temperature stratification is slight. The field is essentially that due to a spherical source and its image in the boundary and, as such, depends strongly on the boundary impedance. However, the results of this study show that within the shadow zone or diffraction region the diminution of the sound intensity with distance is very much greater than that caused by ground and air absorption in a homogeneous atmosphere. In fact, in this region the sound behaves like a damped cylindrical wave, the intensity level of which, apart from cylindrical divergence, decays linearly with distance. The rate of decay has been obtained theoretically in terms of frequency, temperature gradient, and ground impedance. The results, both theoretical and experimental, indicate that the major portion of the sound intensity in the shadow region decays exponentially with distance at a rate proportional to the one-third power of frequency and to the two-thirds power of temperature gradient. The effect of boundary impedance enters mainly through its resistive component. The rate of sound decay for a pressure-release or absorbing boundary (zero impedance) is found to be 2.3 times that for a reflecting boundary (infinite impedance) and for low impedances is largely independent of the reactive component.

Massachusetts Institute of Technology,
Cambridge, Mass., December 12, 1954.

REFERENCES

1. Ingard, Uno: A Review of the Influence of Meteorological Conditions on Sound Propagation. Jour. Acous. Soc. Am., vol. 25, no. 3, May 1953, pp. 405-411.
2. Ingard, Uno: On the Reflection of a Spherical Sound Wave From an Infinite Plane. Jour. Acous. Soc. Am., vol. 23, no. 3, May 1951, pp. 329-335.
3. Sieg, Helmut: Schallausbreitung im Freien. Elektrische Nachrichten Technik, Bd. 17, Heft 9, Sept. 1940, pp. 193-208.
4. Von Wittinghausen, W. G-F.: Ueber Strahlengeometrie in Parallelgeschichteten Medien. Akustische Zs., Bd. 8, Heft 5, Oct. 1943, pp. 175-185.
5. Pekeris, C. L.: Theory of Propagation of Sound in a Half-Space of Variable Sound Velocity Under Conditions of Formation of a Shadow Zone. Jour. Acous. Soc. Am., vol. 18, no. 2, Oct. 1946, pp. 295-315.
6. Courant, R., and Hilbert, D.: Methoden der mathematischen Physik. Vol. I. Julius Springer (Berlin), 1931.
7. Langer, R.: On the Connection Formulas and the Solutions of the Wave Equation. Phys. Rev., vol. 51, no. 8, Apr. 15, 1937, pp. 669-676.
8. Blokhintzev, D. (R. T. Beyer and D. Mintzer, trans.): The Acoustics of an Inhomogeneous Moving Medium. Dept. Phys., Brown Univ., Aug. 1952.
9. Storm, M. L.: Heat Conduction in Simple Metals. Jour. Appl. Phys., vol. 22, no. 7, July 1951, pp. 940-951.
10. Chapman, Sydney, and Cowling, T. G.: The Mathematical Theory of Non-Uniform Gases. Univ. Press (Cambridge), 1939, pp. 169, 172.
11. Stops, D. W.: Effect of Temperature Upon the Thermal Conductivity of Gases. Nature, vol. 164, no. 4179, Dec. 3, 1949, pp. 966-967.

APPENDIX A

APPROXIMATION OF A SLOWLY VARYING MEDIUM

The general linear wave equation is (ref. 8)

$$\frac{\partial^2 \phi}{\partial t^2} = c^2 \nabla^2 \phi + (\nabla \pi_0) \nabla \phi$$

where $\pi_0 = \int \frac{dp}{\rho}$ is the enthalpy. If an adiabatic atmosphere $p = r\rho^\gamma$ is assumed, where γ is the ratio of specific heats and r is a constant, the following equation may be obtained:

$$\pi_0 = r \frac{\gamma}{\gamma - 1} \rho^{(\gamma-1)}$$

Whence, for a stratified medium,

$$\nabla \pi_0 = \frac{d}{dz} \pi_0 = \frac{\gamma p}{\rho} \frac{\rho'}{\rho}$$

Now, $c^2 = \frac{\gamma p}{\rho}$; hence,

$$c' = \frac{1}{2} c (\gamma - 1) \frac{\rho'}{\rho}$$

Thus,

$$\nabla \pi_0 = \frac{2cc'}{\gamma - 1}$$

If it is assumed that $\phi \propto e^{i\omega[t-(z/c)]}$, it follows directly that the condition

$$c^2 \nabla^2 \phi \gg (\nabla \pi_0) \nabla \phi$$

is equivalent to

$$\frac{d\lambda}{dz} \approx \frac{\delta\lambda}{\lambda} \ll 1$$

APPENDIX B

APPROXIMATION TO WAVE EQUATION

To evaluate

$$\theta = \frac{3}{4} \left(\frac{Q'}{Q} \right)^2 - \frac{1}{2} \frac{Q''}{Q} - \frac{5}{36} \left(\frac{Q}{u} \right)^2$$

where

$$Q^2 = \frac{\omega^2}{c^2} - k^2$$

$$u = \int_{z_0}^z Q \, dz$$

$$c = c_0 (1 - z/H)^{1/2}$$

compute first

$$c' = -c_0^2 / 2cH$$

$$c'' = -c_0^4 / 4c^3 H^2$$

$$Q' = \frac{\omega^2 c_0^2}{2c^4 QH}$$

$$Q'' = -\frac{\omega^4 c_0^4}{4c^8 Q^3 H^2} + \frac{\omega^2 c_0^4}{c^6 QH^2}$$

$$u = -(c/c_0)^2 QH + \left(\omega^2 H / c_0^2 k \right) \tan^{-1}(Q/k)$$

When Q/k is small,

$$u \rightarrow \frac{c^2 Q H}{c_o^2 k^2} \left[-k^2 + \frac{\omega^2}{c^2} - \frac{1}{3} \left(\frac{\omega Q}{c k} \right)^2 + \frac{1}{5} \left(\frac{\omega Q^2}{c k^2} \right)^2 + \dots \right]$$

Substitute $k^2 = \frac{\omega^2}{c^2} (1 - \gamma)$ where $\gamma = c^2 Q^2 / \omega^2$. Then,

$$u = \frac{2c^4 Q^3 H}{3c_o^2 \omega^2} \left(1 + \frac{4}{5} \gamma + \frac{9}{10} \gamma^2 + \dots \right)$$

and

$$\left(\frac{Q}{u} \right)^2 = \frac{9}{4} \left(\frac{c_o \omega}{c^2 Q} \right)^4 \frac{1}{H^2} \left(1 - \frac{8}{5} \gamma + \frac{3}{5} \gamma^2 + \dots \right)$$

By combining these, the following equation is obtained:

$$\theta = -(3/16) (c_o/c)^4 / H^2 + O \left(Q c_o^2 / \omega c H \right)^2 + \dots$$

APPENDIX C

SIMPLIFICATION OF EIGENVALUE EQUATION

In order to find the eigenvalues k_m the roots of equation (31) must first be determined. The right-hand side of this equation is

$$\begin{aligned} \frac{dF_m}{dz} &= \frac{d}{dz} \left[\left(\frac{u}{Q} \right)^{1/2} H_{1/3}^{(2)}(u) \right]_{z=0} \\ &= \left[\frac{1}{6} \left(\frac{Q}{u} \right)^{1/2} - \frac{1}{2} \left(\frac{u}{Q} \right)^{1/2} \frac{Q'}{Q} \right]_{z=0} H_{1/3}^{(2)}(u_0) + (u_0 Q_0)^{1/2} H_{-2/3}^{(2)}(u_0) \end{aligned}$$

so that

$$\frac{i\omega\rho}{Z} = \left(\frac{1}{F} \frac{dF}{dz} \right)_{z=0} = \frac{1}{6} \frac{Q_0}{u_0} - \frac{1}{2} \frac{Q_0'}{Q_0} + Q_0 \frac{H_{-2/3}^{(2)}(u_0)}{H_{1/3}^{(2)}(u_0)} \quad (45)$$

where the primes denote differentiation with respect to z . As was shown in appendix B, the values of Q/u given in equations (32) and (33) may be expanded in terms of the small quantity γ_0 as

$$Q_0/u_0 = \left(3\omega^2/2c_0^2 Q_0^2 H \right) \left(1 - \frac{4}{5} \gamma_0 - \frac{13}{50} \gamma_0^2 - \dots \right)$$

where

$$\gamma_0 = (c_0 Q_0/\omega)^2 = (3c_0 u_0/2\omega H)^{2/3}$$

Furthermore,

$$Q_0'/Q_0 = \frac{1}{2} \left(\omega^2/c_0^2 Q_0^2 H \right)$$

from which it follows that

$$\left(\frac{1}{F_m} \frac{dF_m}{dz} \right)_{z=0} \approx -\frac{1}{5} H + Q_0 \frac{H_{-2/3}^{(2)}(u_0)}{H_{1/3}^{(2)}(u_0)}$$

Since the first term on the right side is very small compared with the second, it is justifiable to approximate equation (45) by

$$\frac{J_{1/3}(v_m) + J_{-1/3}(v_m)}{J_{2/3}(v_m) - J_{-2/3}(v_m)} = \frac{-iZQ_0}{\omega \rho_0} \quad (v_m = u_0 e^{-i\pi}) \quad (46)$$

The last step follows from the relations

$$H_\nu^{(2)}(z) = (i/\sin \nu\pi) [J_{-\nu}(z) - J_\nu(z)e^{i\nu\pi}]$$

$$J_\nu(ze^{-i\pi}) = e^{-i\nu\pi} J_\nu(z)$$

Now, $Q_0^2 = \left[(\omega^2/c_0^2) - k^2 \right]^{1/2}$ is itself a function of v_m through equation (33) taken at $z = 0$. With the substitution $Q_0 = k \tan \tau$ it follows that

$$Q_0 = (\omega/c_0) \sin \tau \quad (47)$$

which together with equation (46) gives equation (35).

APPENDIX D

TEMPERATURE DISTRIBUTION IN A RECTANGULAR ENCLOSURE

The steady-state heat-flow equation is

$$\text{div}[\lambda(T) \text{ grad } T] = 0 \quad (48)$$

where $\lambda(T)$ is the conductivity and T , the temperature. This equation is nonlinear and is not easily solved directly. Storm (ref. 9) has shown in a study of heat conduction in metals that in the one-dimensional case it can be linearized provided that

$$\frac{1}{\sqrt{\lambda \rho c_p}} \frac{d}{dT} \log \sqrt{\frac{\rho c_p}{\lambda}}$$

is constant, where ρ is the density and c_p , the specific heat at constant pressure. However, this condition does not seem to be satisfied in the case of a gas for any reasonable choice of $\lambda(T)$.

Kinetic theory based on a rigid-sphere model predicts that for molecules repelling each other as the inverse v th power of the distance the coefficients of viscosity and heat conduction should vary as T^s ,

where $s = \frac{1}{2} + \frac{2}{v-1}$ (ref. 10). This type of dependence is in good

agreement with experimental results obtained by Stops (ref. 11) who measured the thermal conductivity of air over a wide temperature range

(0° to 1,000° C). Accordingly, put $\lambda = \lambda_0 \left(\frac{T}{T_0} \right)^s$ in the equation (48)

to obtain

$$\nabla^2 T + \frac{s}{T} (\text{grad } T)^2 = 0 \quad (49)$$

It is recognized that this equation can be linearized by the transformation

$$T = \tau^{\frac{1}{s+1}} \quad (50)$$

so that

$$\nabla^2 \tau = 0 \quad (51)$$

In the experimental setup the high temperature is on the top of the chamber in order to diminish the effect of convection of air which is disregarded here. Furthermore, radiation is neglected by assuming that $\sigma T^4 \ll \lambda_M \text{ grad } T$ (σ , Stefan-Boltzmann constant; λ_M , conductivity of the metal). Moreover, since the ratio of the conductivity of metal to air is on the order of 5,000 for steel, the heat transfer between the air and the side walls will have a negligible effect on the temperature distribution. To a first approximation, the temperature gradient within the side walls can therefore be assumed to be constant. The problem is then to find a solution to equation (49) satisfying the boundary conditions $T(x,0) = T_0$ and $T(\frac{+L}{2}, y) = T_0 - \beta y$. If the variables are changed as

$$\tau^{1/(s+1)}(x,y) = \frac{T(x,y)}{T_0}$$

the problem reduces to that of obtaining a solution to Laplace's equation in a bounded two-dimensional region, $-\frac{L}{2} \leq x \leq \frac{L}{2}$, $0 \leq y \leq T_0/\beta$, the

boundary conditions now being $\tau(x,0) = 1$, $\tau(x, T_0/\beta) = 0$, and

$$\tau(\frac{+L}{2}, y) = (\beta y/T_0)^{s+1}$$

Set $\tau(x,y)$ equal to a linear combination of functions $\tau_1(x,y) + \tau_2(x,y)$, where τ_1 and τ_2 are separate solutions to Laplace's equation satisfying the boundary conditions, $\tau_1(x,0) = 1$, $\tau_1(x, T_0/\beta) = \tau_1(\frac{+L}{2}, y) = 0$ and $\tau_2(x,0) = \tau_2(x, T_0/\beta) = 0$,

$\tau_2(\frac{+L}{2}, y) = (\beta y/T_0)^{s+1}$ Expressing the solution as a Fourier series in the usual way gives

$$\tau_1 = \frac{4}{\pi} \sum_{m=0}^{\infty} \frac{(-1)^m}{2m+1} \frac{\sinh(2m+1)\pi\gamma\eta}{\sinh(2m+1)\pi\gamma} \cos(2m+1)(\pi x/L) \quad (52)$$

$$\tau_2 = 2 \sum_{m=0}^{\infty} \int_0^1 x^{s+1} \sin m\pi x \, dx \frac{\cosh(m\pi\beta x/T_0)}{\cosh(m\pi/2\gamma)} \sin m\pi\eta \quad (53)$$

where

$$\frac{T_0}{\beta L} = \gamma$$

$$\frac{\beta y}{T_0} = 1 - \eta$$

Use of the identities,

$$\frac{e^y - e^{-y}}{e^{\gamma} - e^{-\gamma}} = e^{-\gamma+y} e^{-\gamma} \frac{\sinh(\gamma - y)}{\sinh \gamma}$$

and

$$\sum_{m=0}^{\infty} \frac{(-1)^m}{2m+1} \operatorname{Re} \left[e^{-(2m+1)(a+ib)} \right] = \frac{1}{2} \tan^{-1} \left(\frac{\cos b}{\sinh a} \right)$$

where Re indicates "real part of," improves the convergence of τ_1 , which then becomes

$$\tau_1 = \frac{4}{\pi} \left\{ \frac{1}{2} \tan^{-1} \left[\frac{\cos \pi x/L}{\sinh \pi \gamma (1 - \eta)} \right] - \sum_{m=0}^{\infty} \frac{(-1)^m e^{-(2m+1)\pi\gamma}}{2m+1} \frac{\sinh(2m+1)\pi\gamma(1-\eta)}{\sinh(2m+1)\pi\gamma} \cos(2m+1)(\pi x/L) \right\}$$

At $x = 0$,

$$\tau_1(0, \eta) = \frac{4}{\pi} \left[\tan^{-1} e^{-\pi\gamma(1-\eta)} - \sum_{m=0}^{\infty} \frac{(-1)^m e^{-(2m+1)\pi\gamma}}{2m+1} \frac{\sinh(2m+1)\pi\gamma(1-\eta)}{\sinh(2m+1)\pi\gamma} \right]$$

In the case of τ_2 it is readily verified that the value of the integral which appears in the Fourier coefficients does not depend critically on the value of s for $n > 2$ provided $0 \leq s \leq 1$. Accordingly, $s = 0$ may be taken for $n > 2$ and the integral may be evaluated by Simpson's rule for $n = 1$ and $n = 2$ with $s = 0.75$. Then, for τ_2 at $x = 0$, the following equation is obtained:

$$\tau_2 = \frac{2}{\pi} \left[0.656 \frac{\sin \pi \eta}{\cosh(\pi/2\gamma)} - 0.512 \frac{\sin 2\pi \eta}{\cosh(\pi/\gamma)} + \sum_{m=3}^{\infty} \frac{(-1)^{m+1}}{m} \frac{\sin m\pi \eta}{\cosh(m\pi/2\gamma)} \right]$$

Figure 8 shows curves of $T = (\tau_1 + \tau_2)^{1/(s+1)}$ for different values of the parameter $\gamma = T_0/\beta L$. The curve labeled $\gamma = 0$ corresponds to the case in which the side walls have been removed to infinity and is equivalent to a situation in which the side walls are replaced by nonconductors.

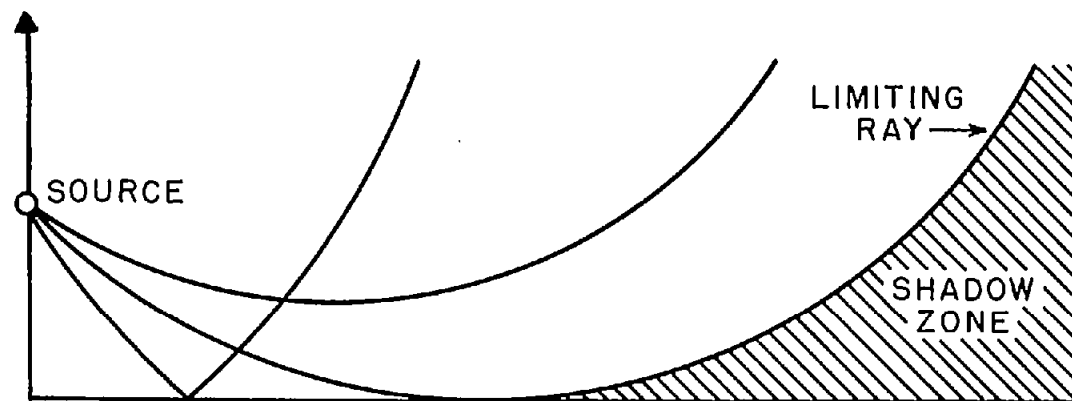


Figure 1.- Illustration of mechanism of shadow-zone formation.

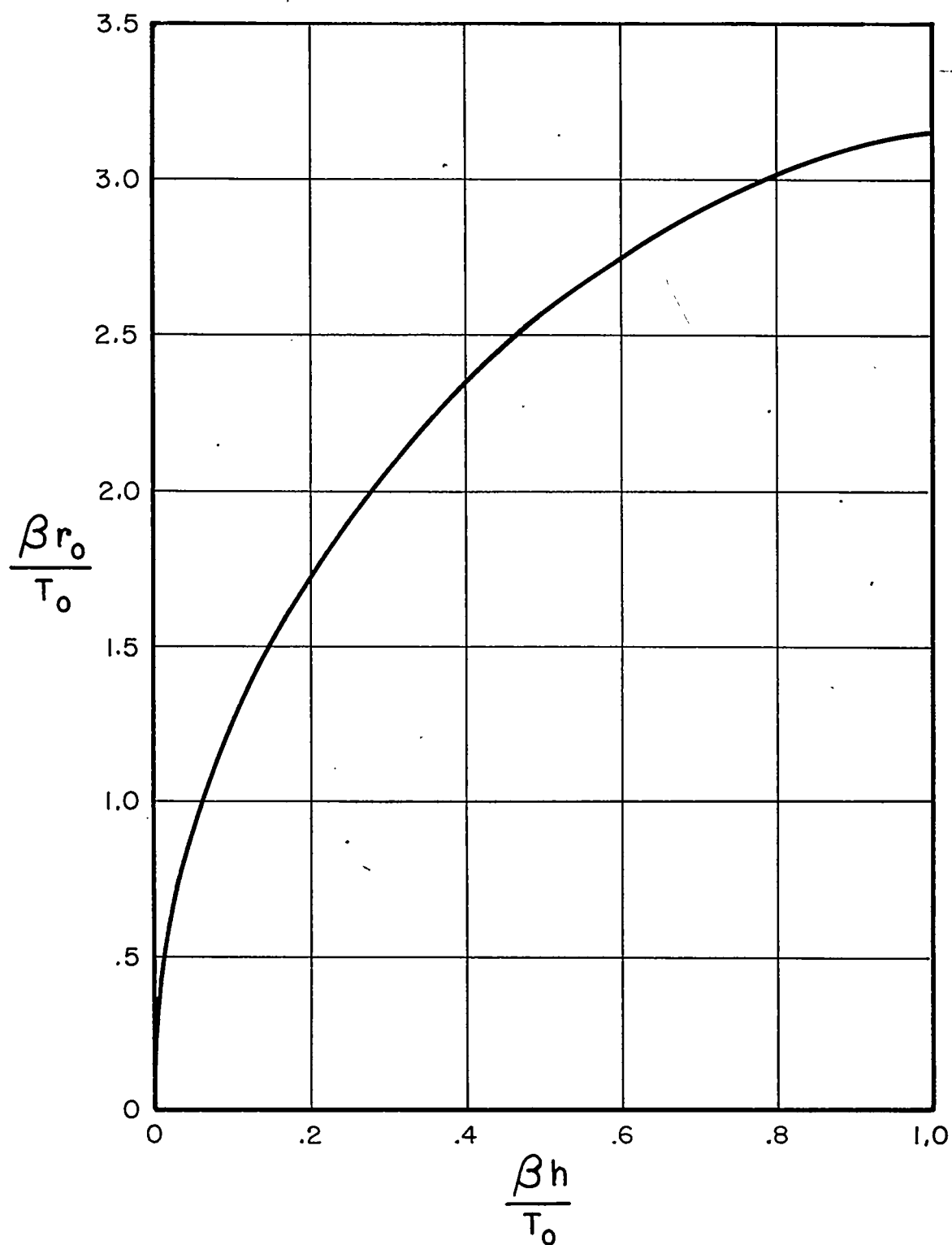


Figure 2.- Distance r_0 to shadow-zone boundary at source height h in temperature gradient β . Temperature at ground is T_0 ($^{\circ}\text{K}$).

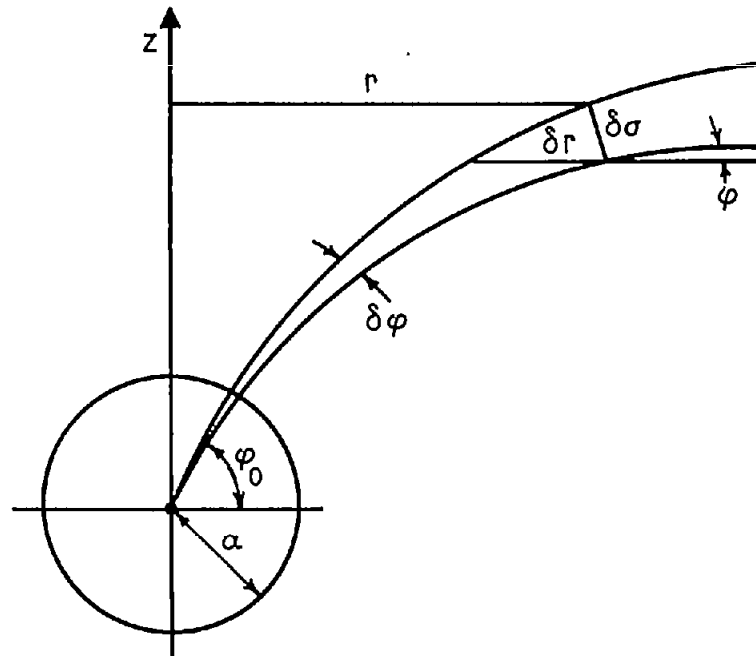


Figure 3.- Ray diagram illustrating computation of intensity distribution around a source in a stratified medium by considering geometrical divergence of rays.

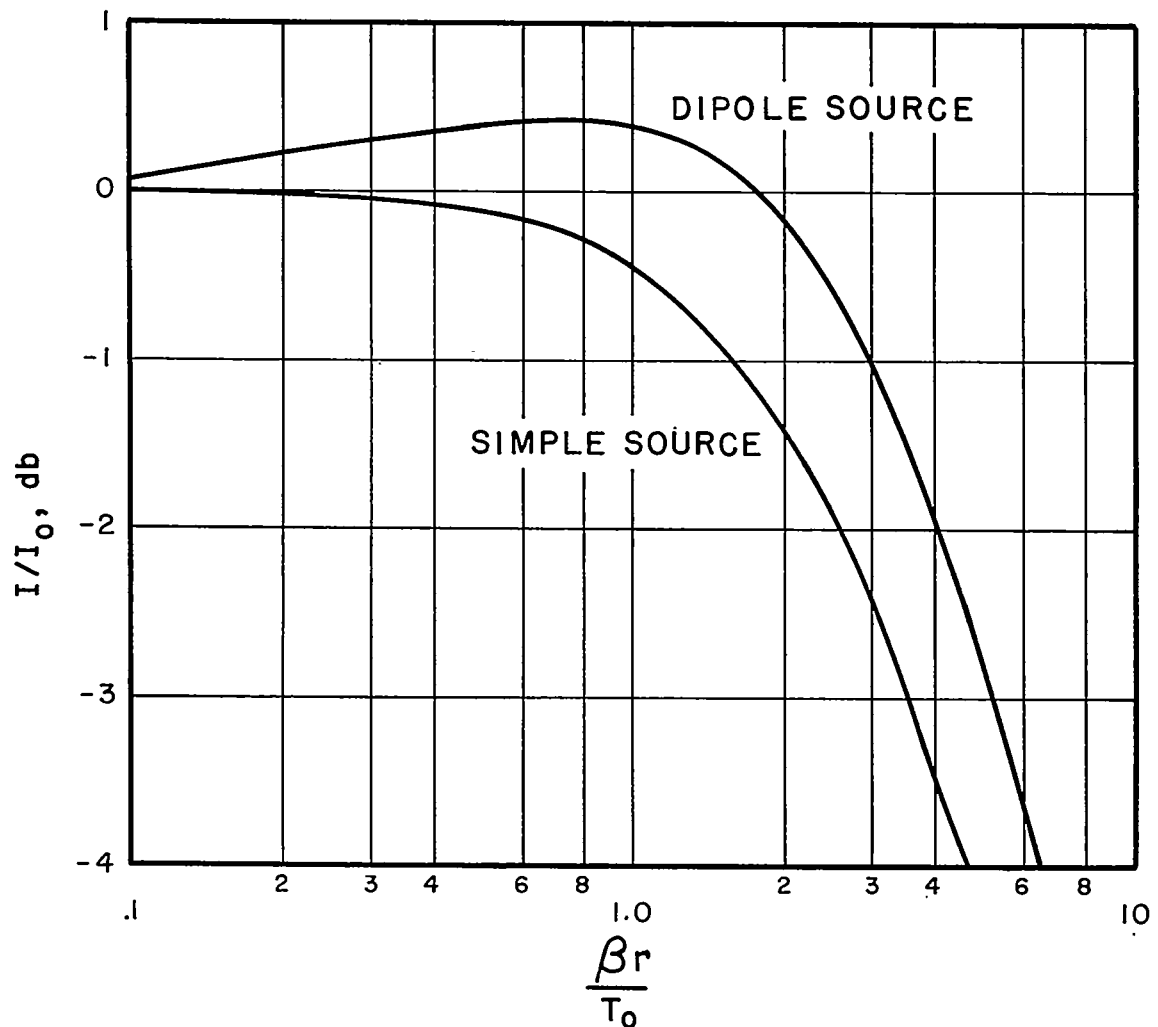


Figure 4.- Computed intensity I from a spherical and a dipole source in temperature gradient β referred to intensity I_0 from same sources in homogeneous medium plotted versus distance parameter $\beta r/T_0$. T_0 is absolute temperature at source elevation.

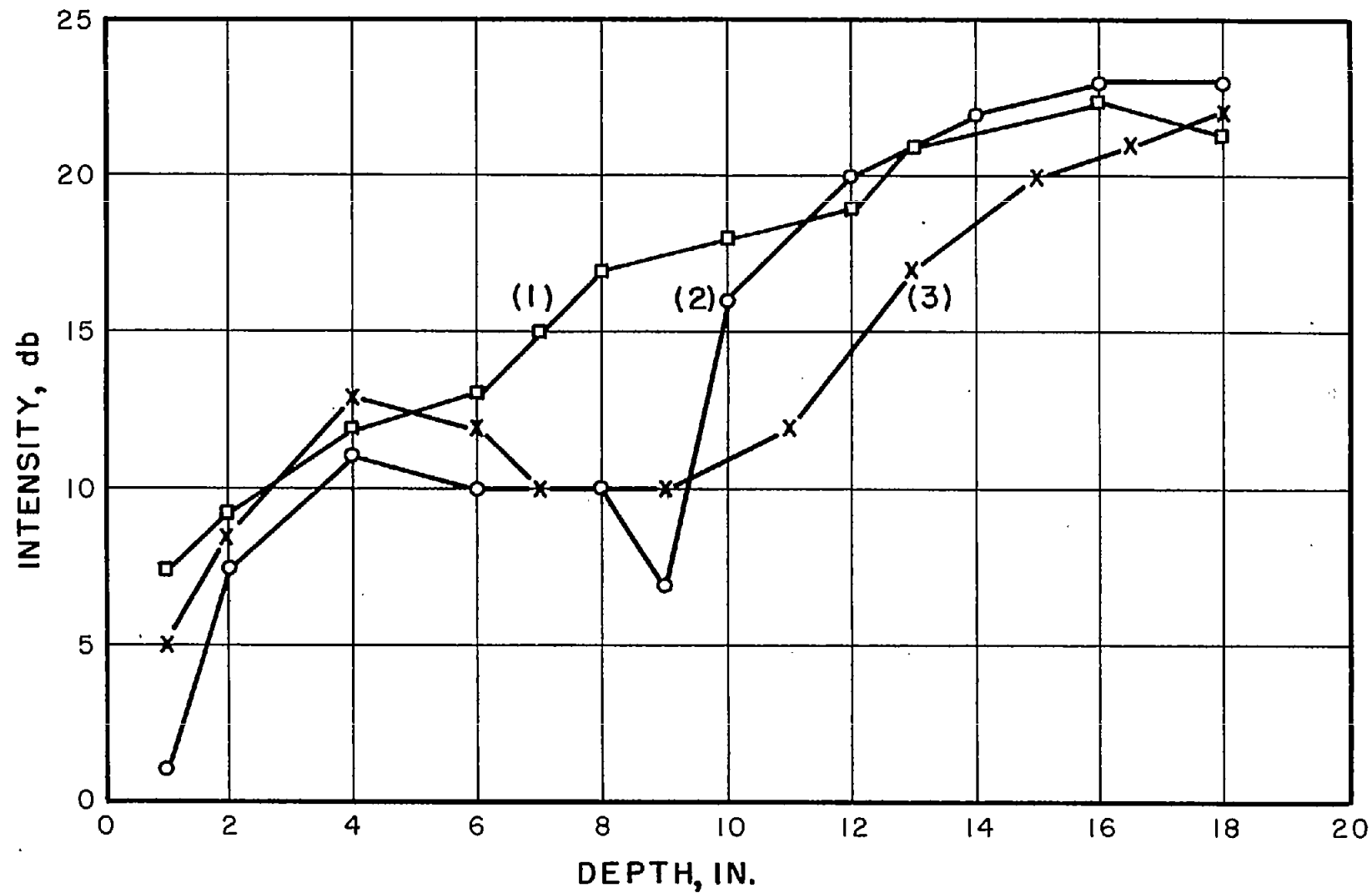


Figure 5.- Intensity level in three-dimensional chamber plotted versus depth from hot surface at distances of (1) 6 feet, (2) 6 feet 6 inches, and (3) 7 feet from speaker.

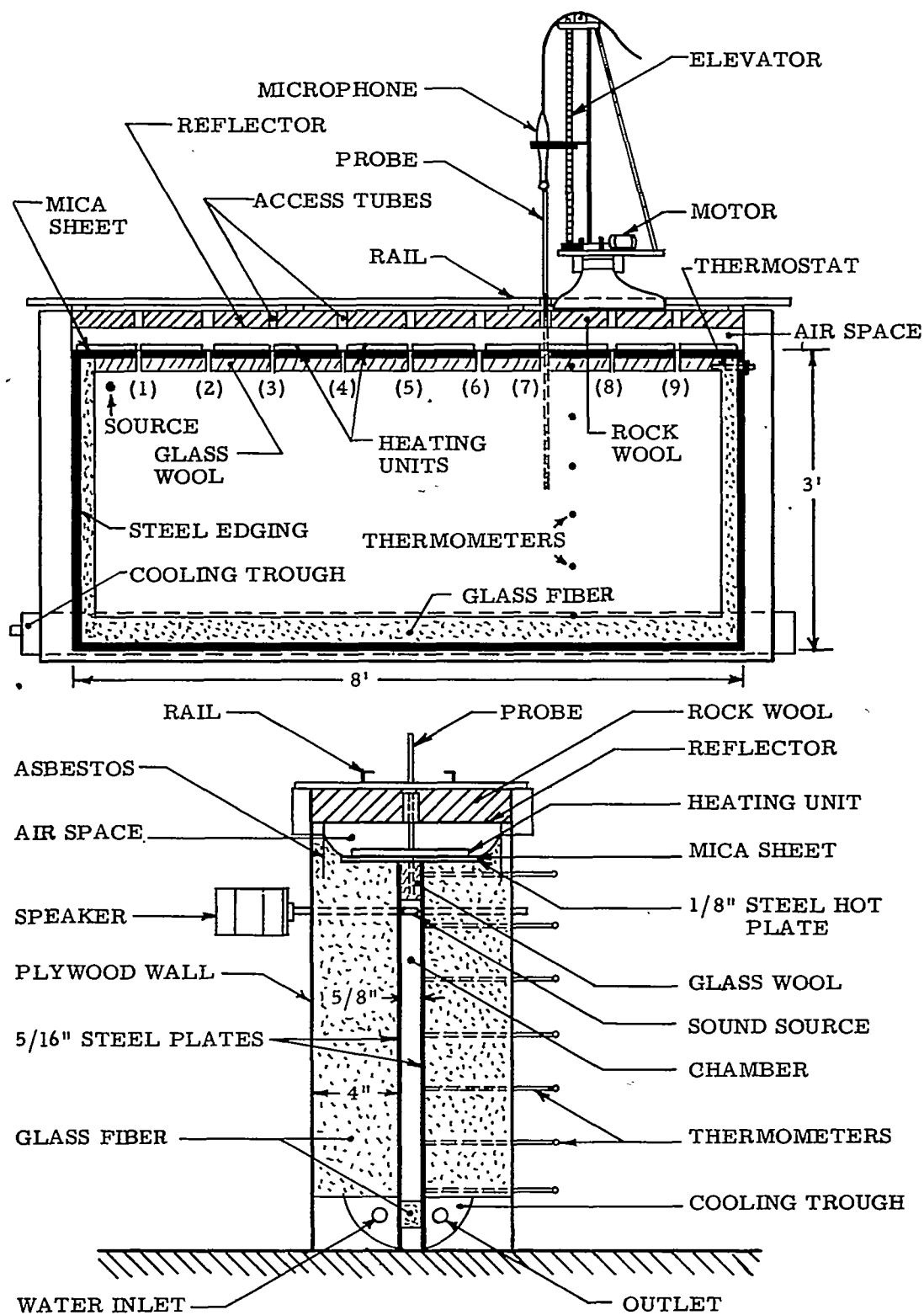


Figure 6.- Schematic views of two-dimensional propagation chamber.

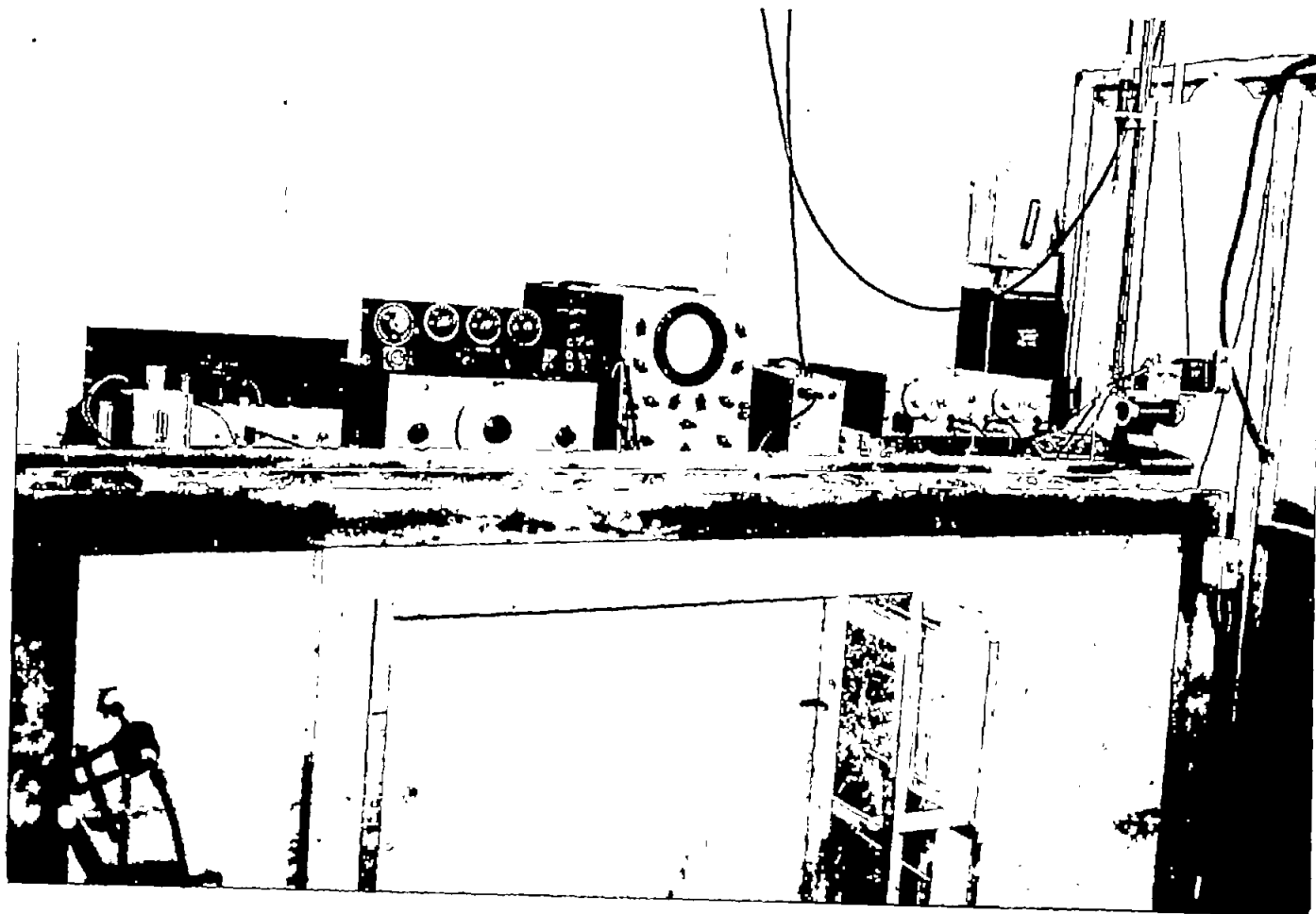


Figure 7.- Photograph of two-dimensional propagation chamber and electronic equipment. L-89374

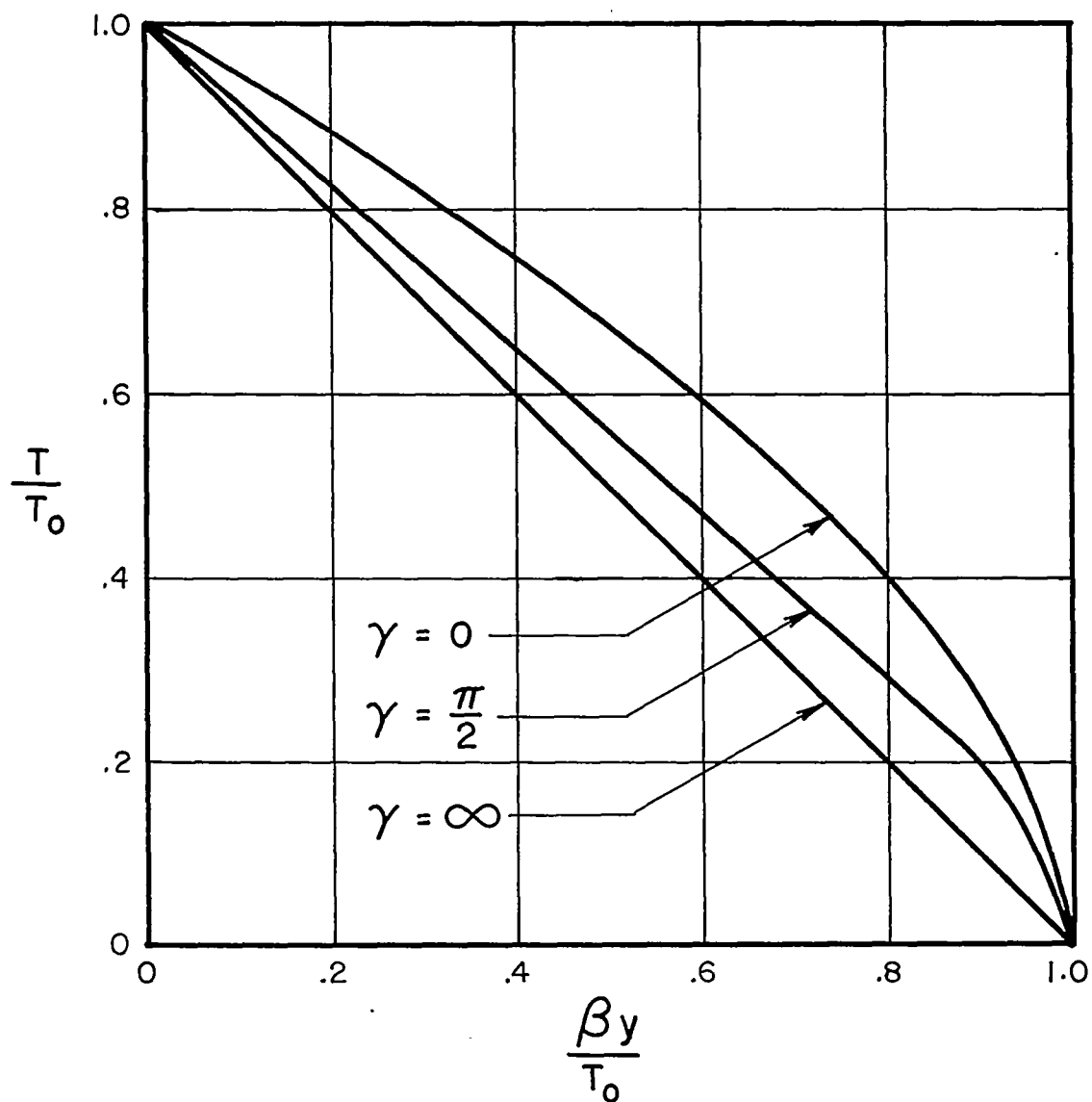


Figure 8.- Absolute temperature ratio T/T_0 in air midway between two vertical side walls in which a constant temperature gradient β exists plotted versus height parameter $\beta y/T_0$ for different separations $L = T_0/\beta y$ of side walls.

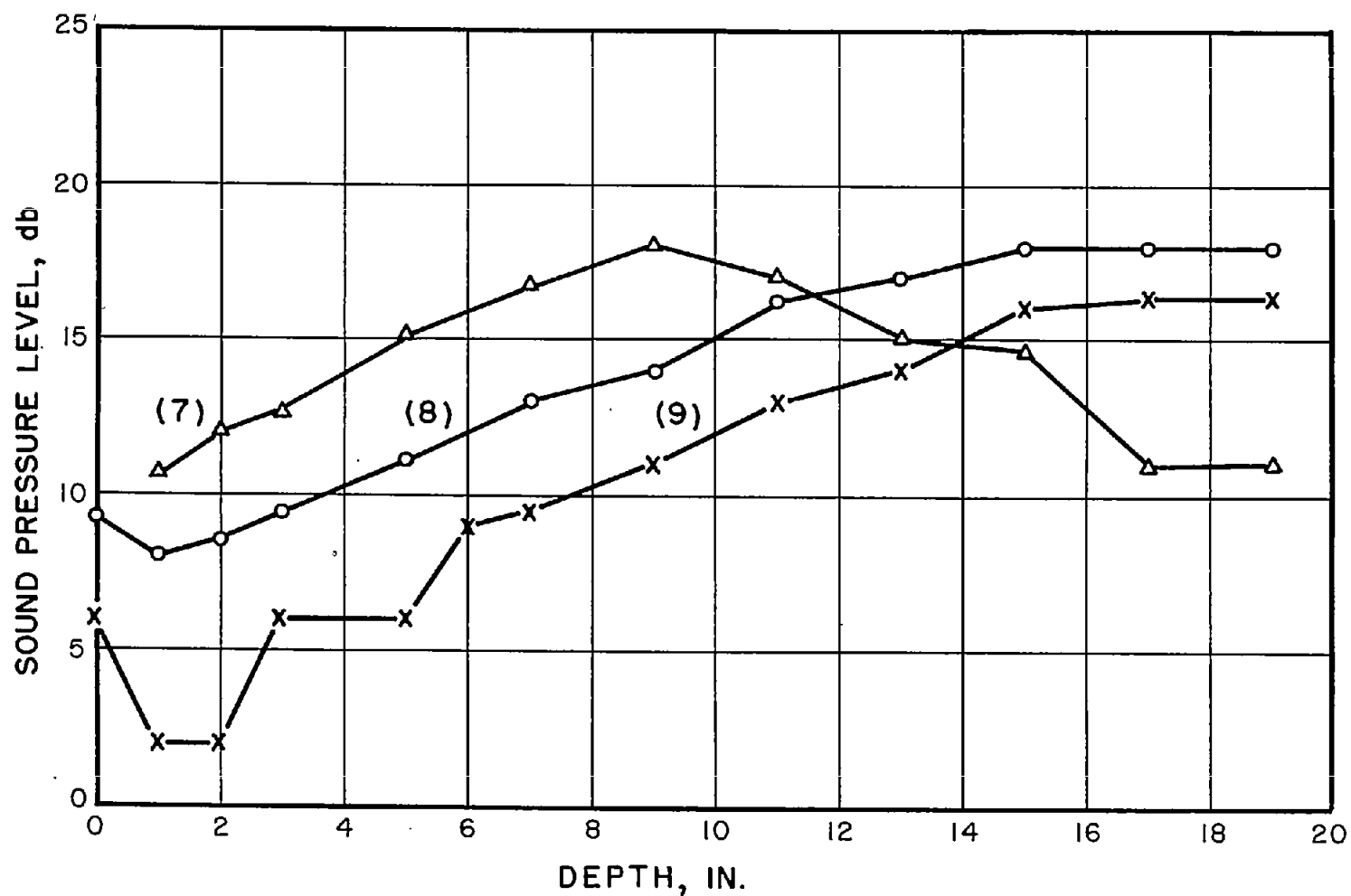


Figure 9.- Measured sound pressure level as a function of depth from a hard boundary taken in chamber in presence of a temperature gradient at (7) 66 inches, (8) 76 inches, and (9) 86 inches from speaker which is driven by 9,250-cps millisecond pulses.

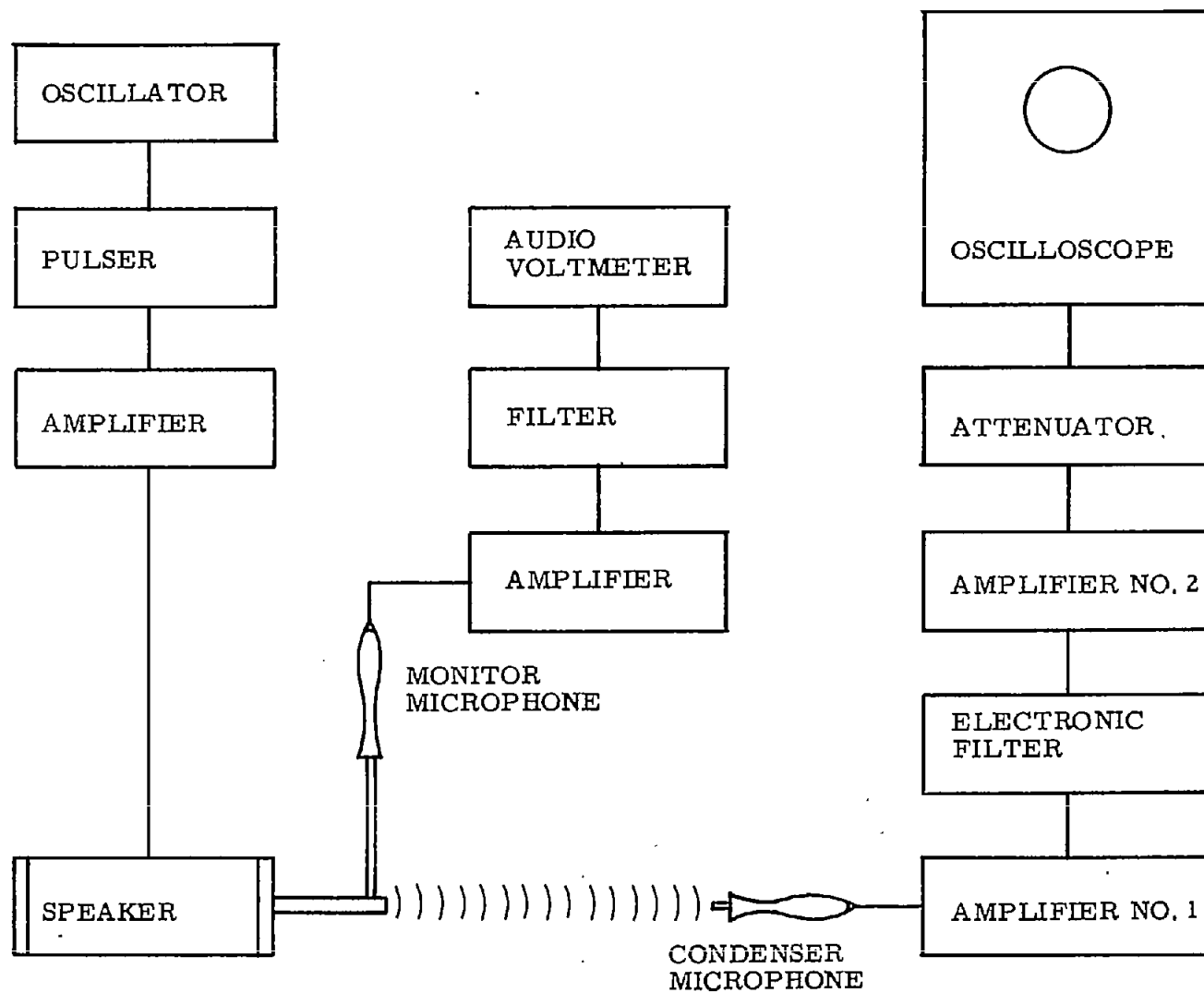


Figure 10.- Block diagram of electronic setup.

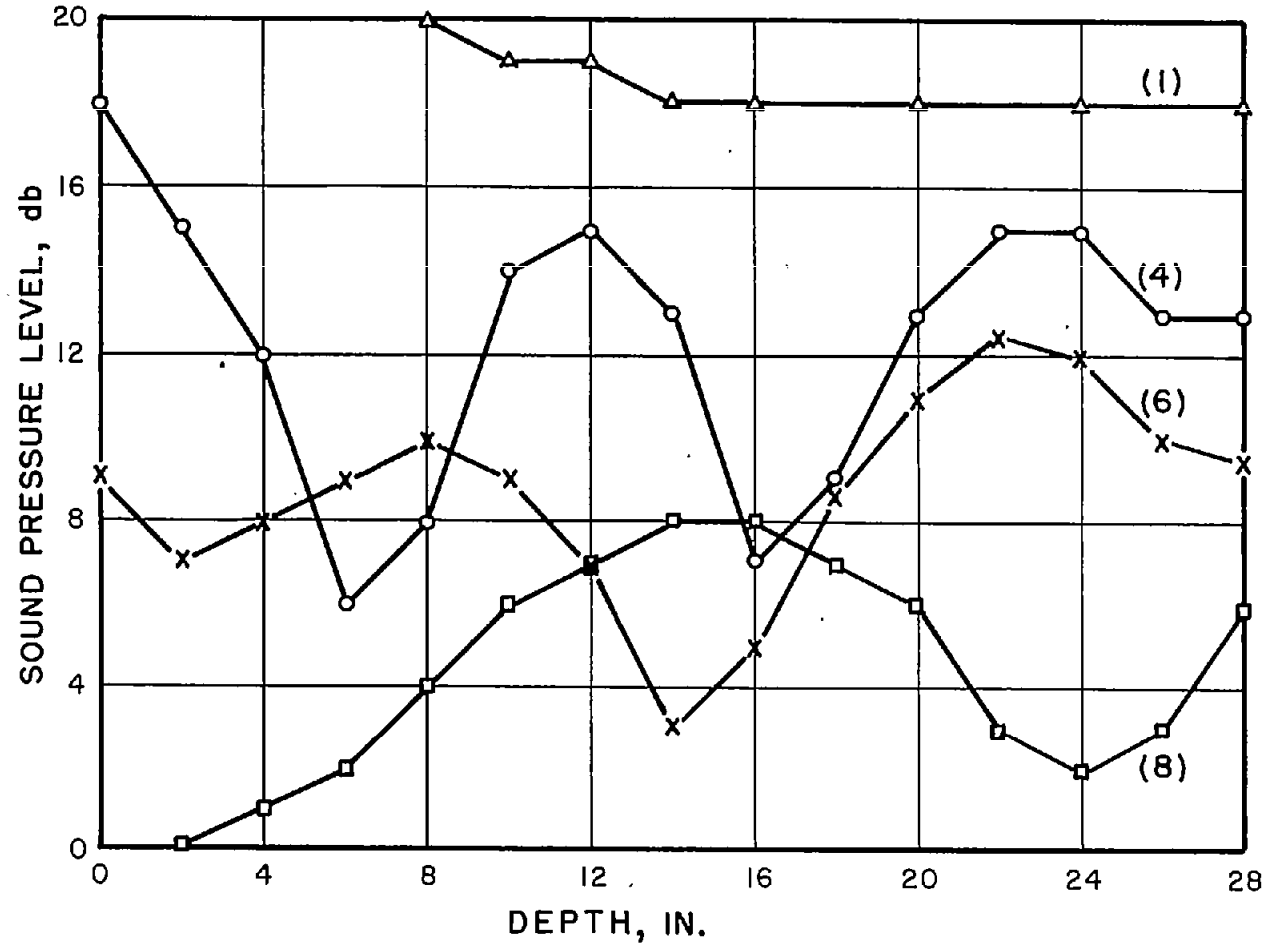
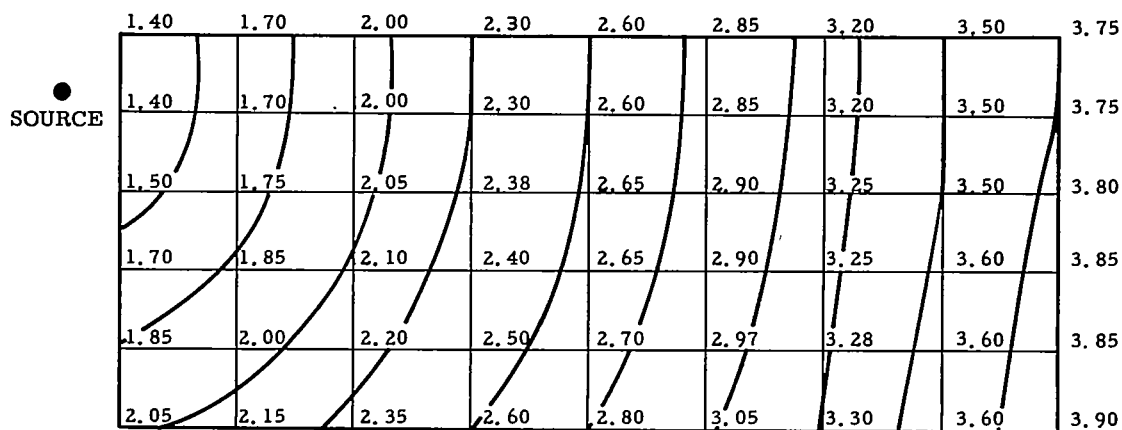


Figure 11.- Measured sound pressure level as a function of depth from a hard boundary taken in chamber at (1) 4 inches, (4) 35 inches, (6) 55 inches, and (8) 76 inches from speaker, which was driven by 8,000-cps millisecond pulses. Temperature gradient was about 210° C per meter.



(a) Without a temperature gradient.

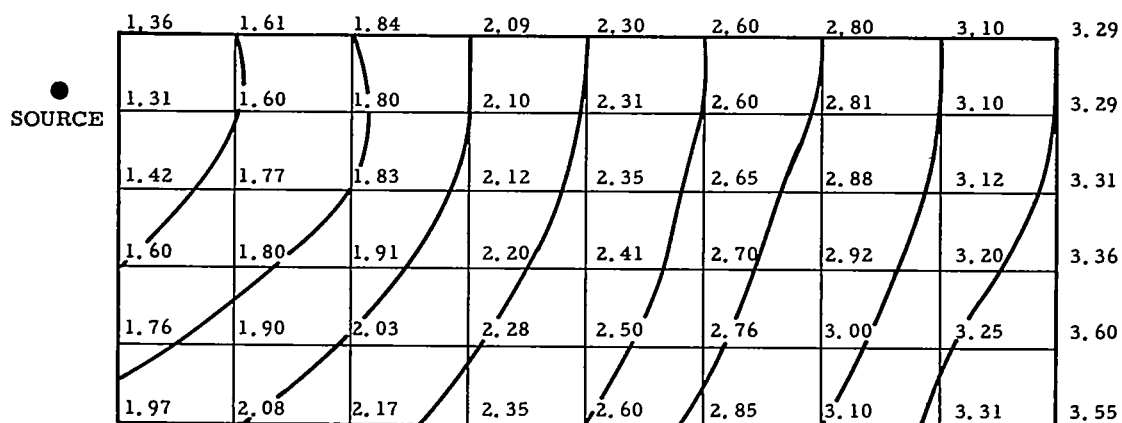
(b) With a temperature gradient of 210° C per meter.

Figure 12.- Surfaces of constant phase in two-dimensional propagation chamber.

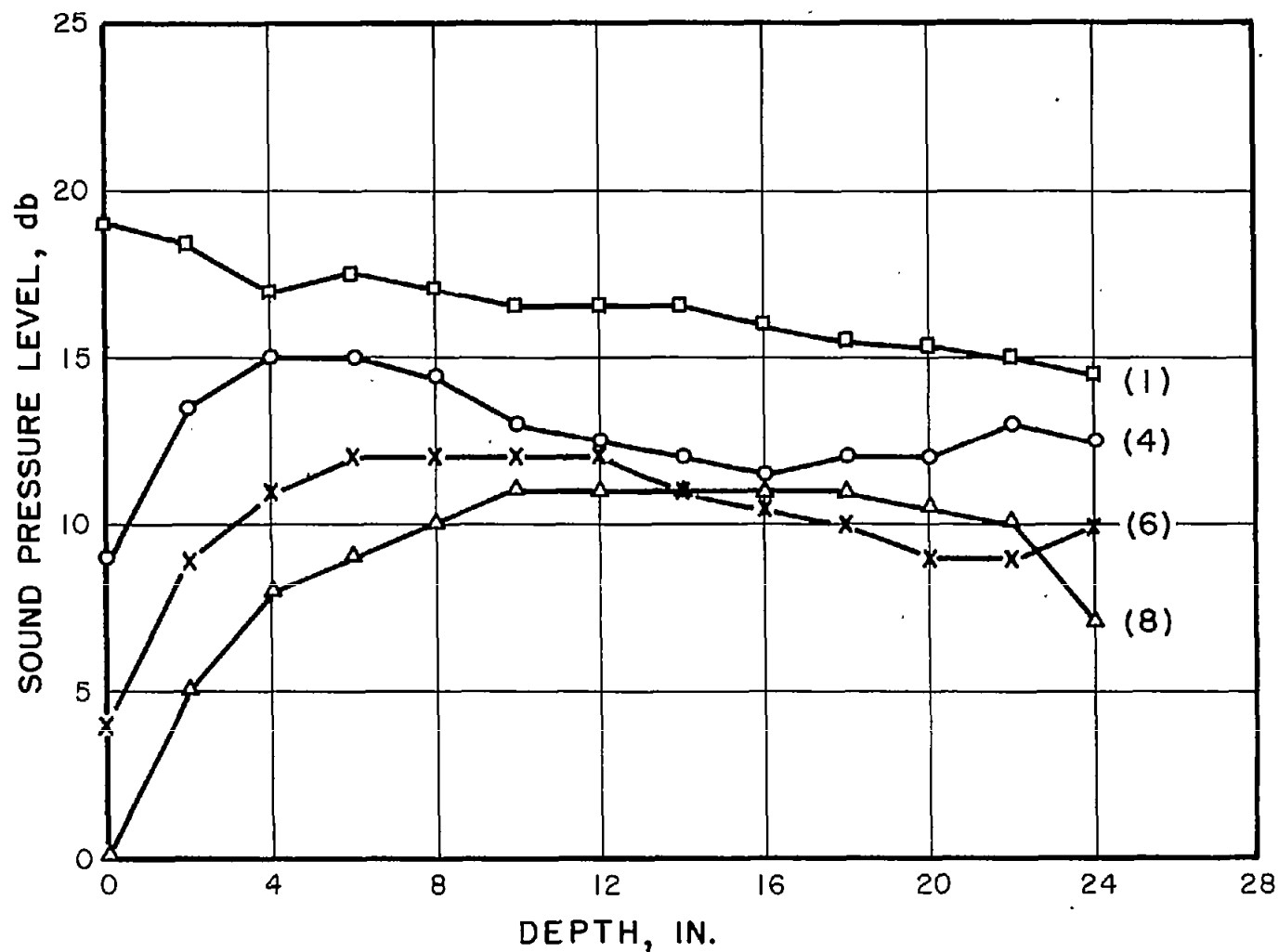


Figure 13.- Measured sound pressure level as function of depth from absorbing boundary taken in chamber at (1) 4 inches, (4) 35 inches, (6) 55 inches, and (8) 76 inches from speaker which was driven by 8,000-cps millisecond pulses. Temperature gradient was about 210°C per meter.

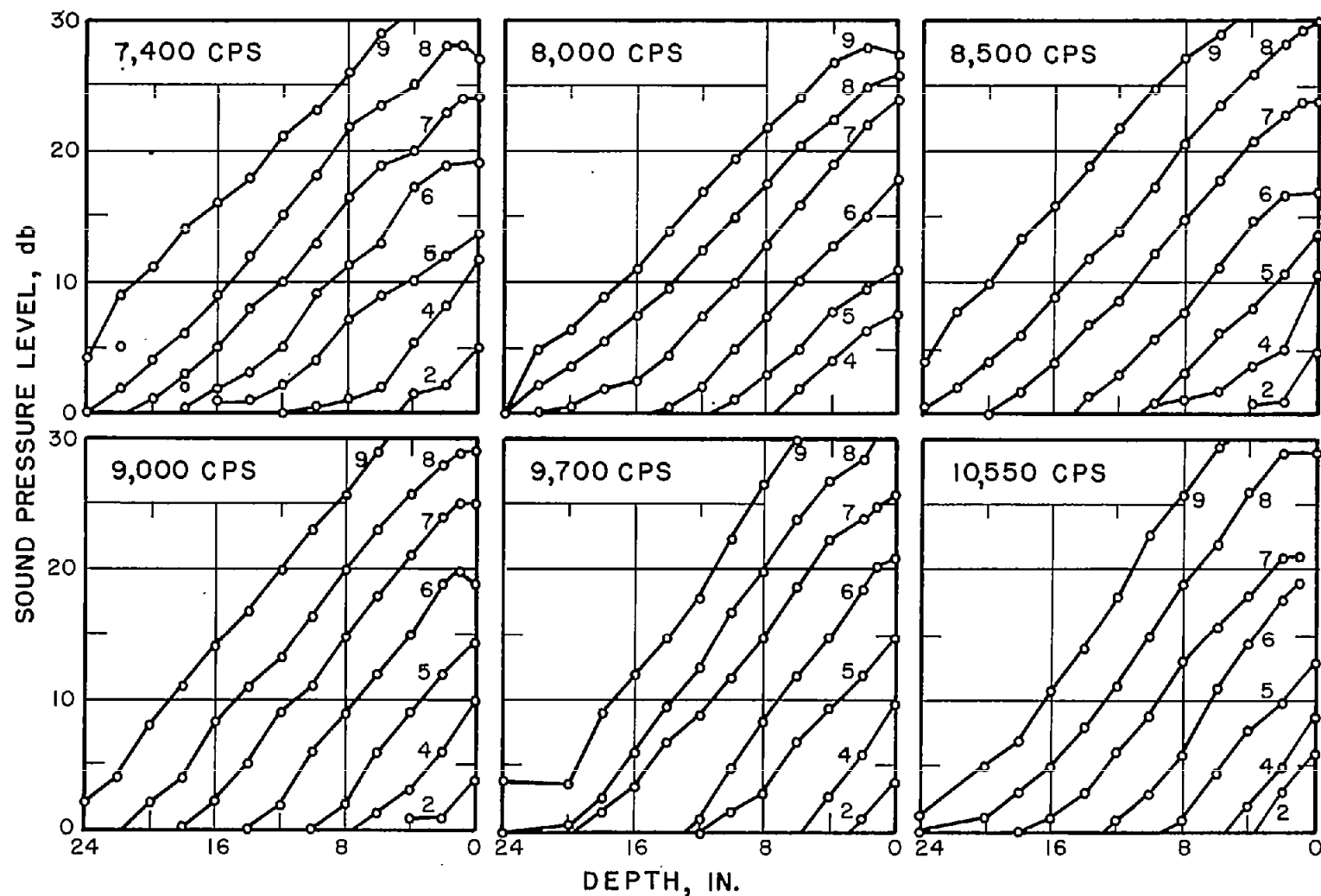


Figure 14.- Additional attenuation brought about by presence of temperature gradient plotted for different frequencies as a function of depth. Numbers on curves correspond to distances from speaker shown in figure 7.

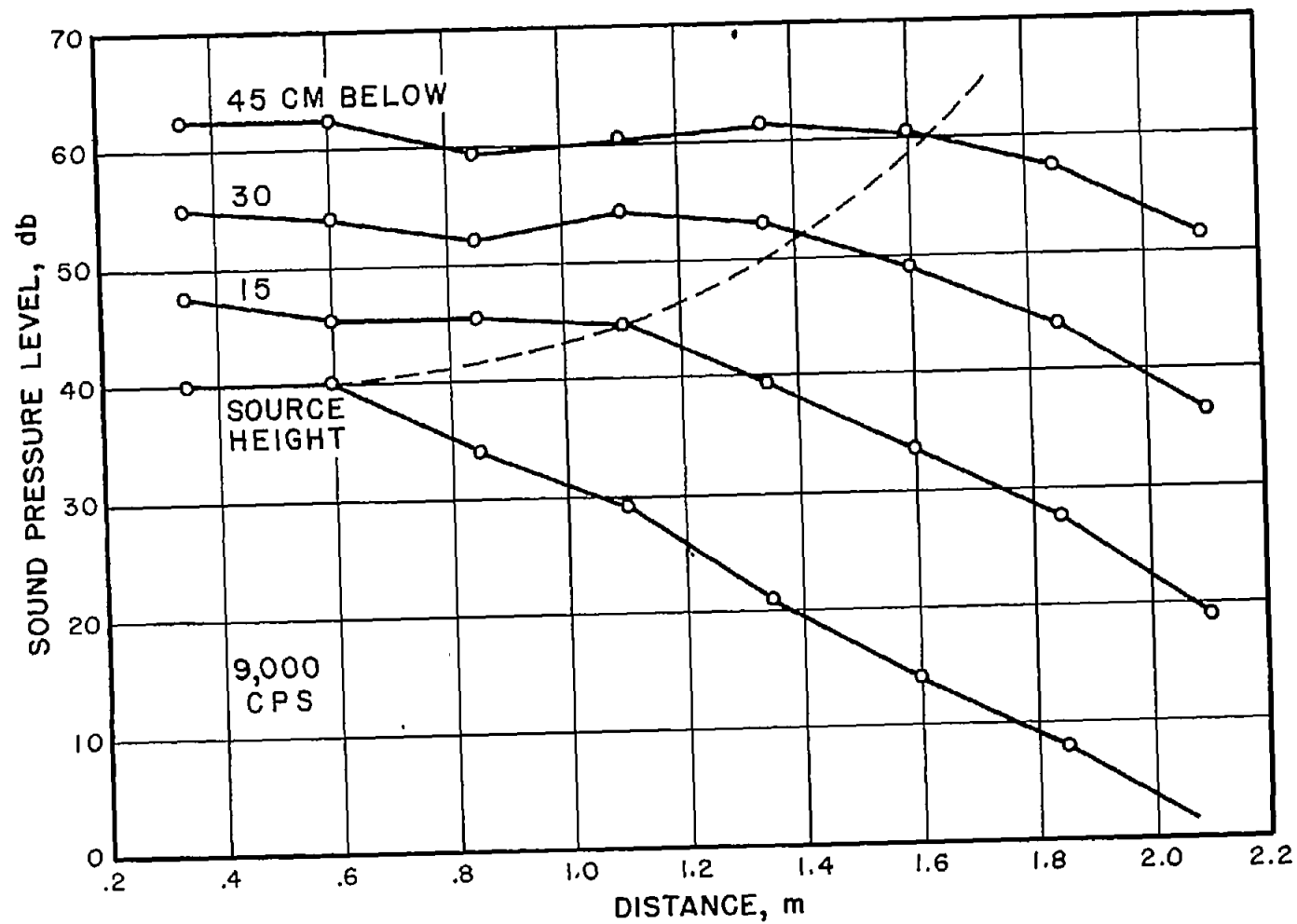


Figure 15.- Measured sound pressure levels at various depths in chamber as a function of horizontal distance from speaker driven by 9,000-cps millisecond pulses over absorbing boundary with vertical temperature gradient. Dashed curve indicates shadow-zone boundary.

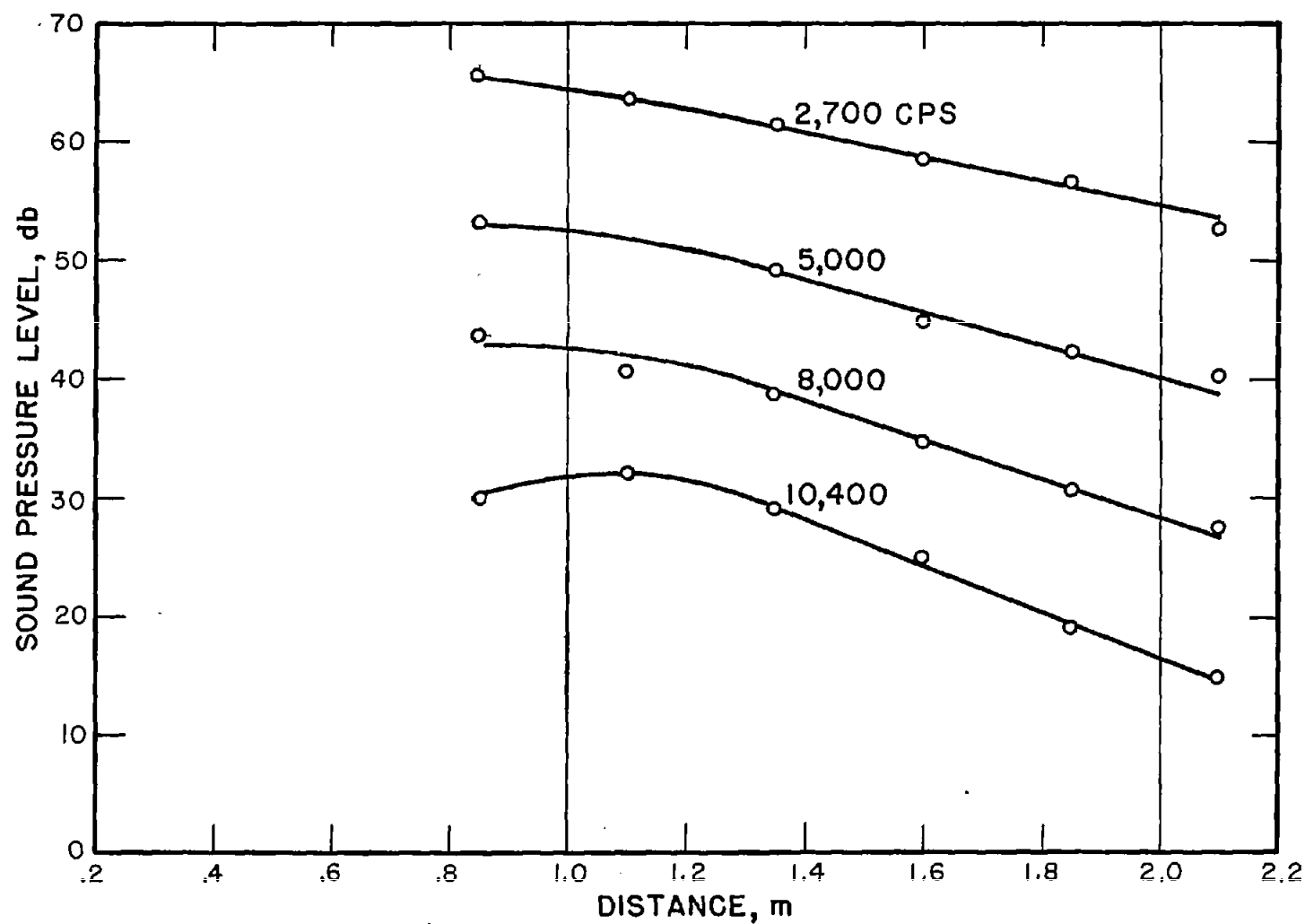


Figure 16.- Measured sound pressure level as a function of horizontal distance from source over a hard boundary with a vertical temperature gradient.

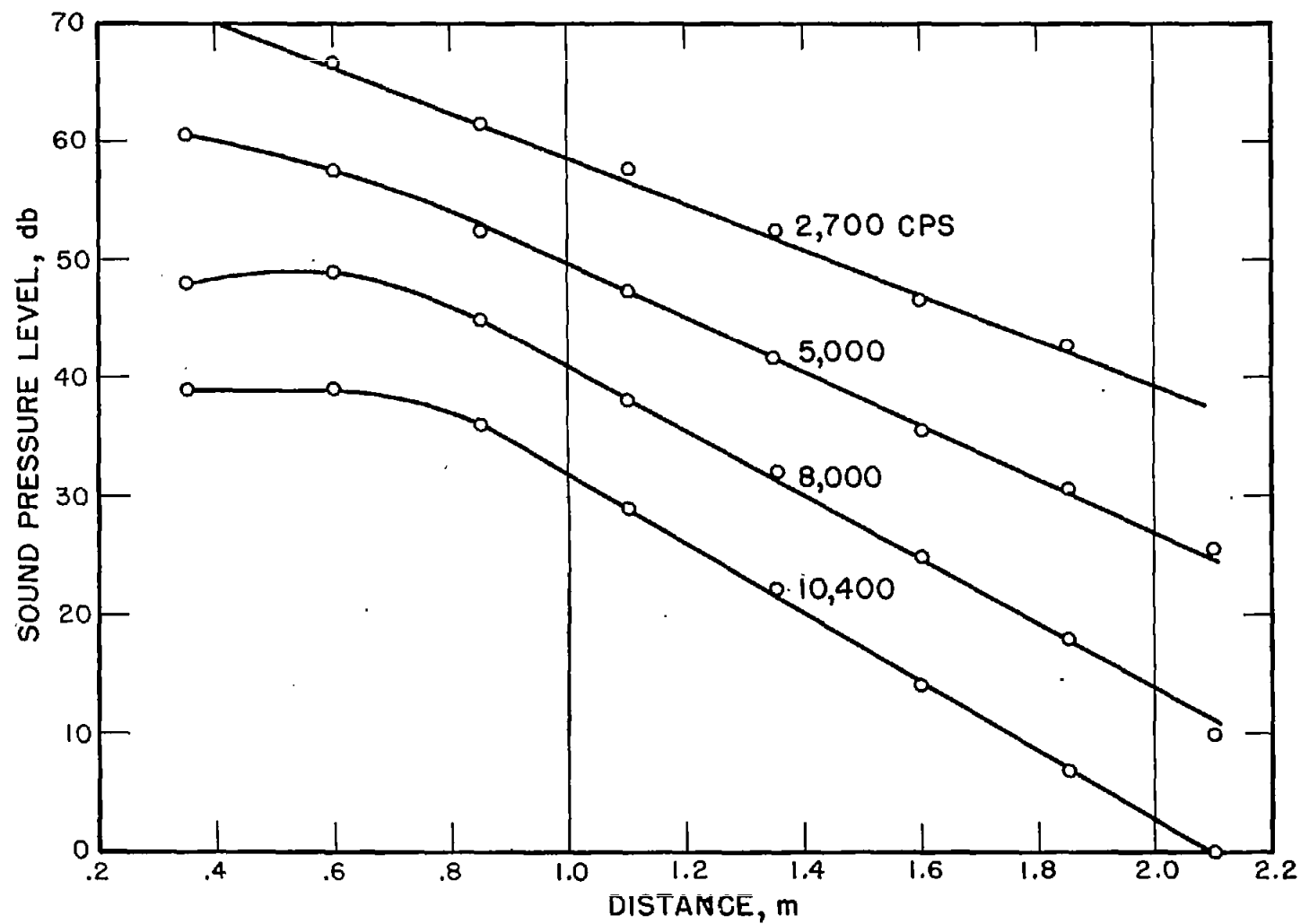


Figure 17.- Measured sound pressure level as a function of horizontal distance from source over absorbing boundary with a vertical temperature gradient.

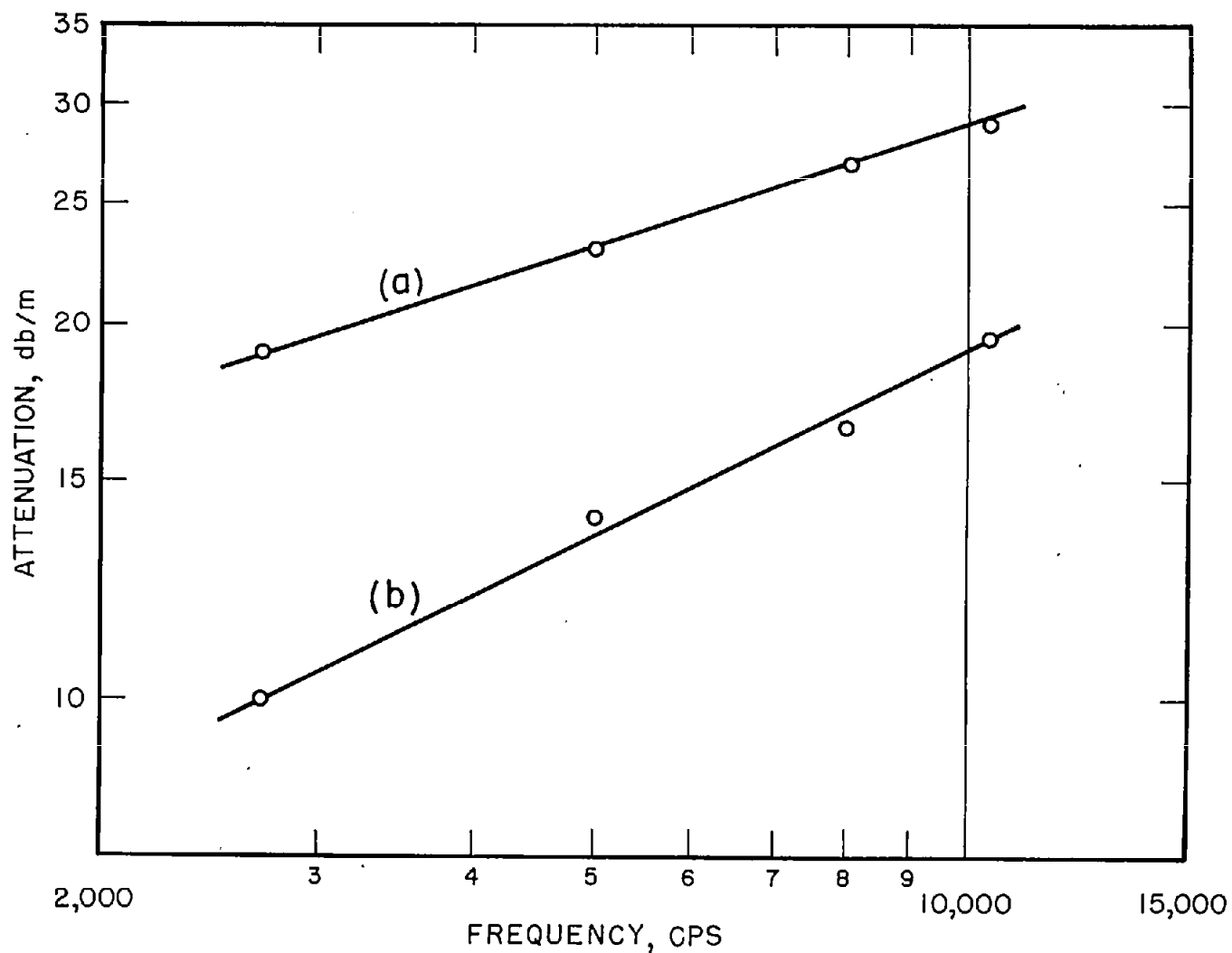


Figure 18.- Measured attenuation in shadow zone as function of frequency.
 (a) indicates soft boundary; (b) indicates hard boundary.